

## **LiDAR point-cloud mapping of building façades for building energy performance simulation**

O'Donnell, J.; Truong-Hong, Linh; Boyle, N.; Corry, Edward; Cao, Jun; Laefer, Debra F.

**DOI**

[10.1016/j.autcon.2019.102905](https://doi.org/10.1016/j.autcon.2019.102905)

**Publication date**

2019

**Document Version**

Accepted author manuscript

**Published in**

Automation in Construction

**Citation (APA)**

O'Donnell, J., Truong-Hong, L., Boyle, N., Corry, E., Cao, J., & Laefer, D. F. (2019). LiDAR point-cloud mapping of building façades for building energy performance simulation. *Automation in Construction, 107*, Article 102905. <https://doi.org/10.1016/j.autcon.2019.102905>

**Important note**

To cite this publication, please use the final published version (if applicable). Please check the document version above.

**Copyright**

Other than for strictly personal use, it is not permitted to download, forward or distribute the text or part of it, without the consent of the author(s) and/or copyright holder(s), unless the work is under an open content license such as Creative Commons.

**Takedown policy**

Please contact us and provide details if you believe this document breaches copyrights. We will remove access to the work immediately and investigate your claim.

# LiDAR point-cloud mapping of building façades for building energy performance simulation

James O'Donnell<sup>a</sup>, Linh Truong-Hong<sup>b</sup>, Niamh Boyle<sup>a</sup>, Edward Corry<sup>a,e</sup>,  
Jun Cao<sup>d</sup>, Debra F. Laefer<sup>c,f</sup>

<sup>a</sup>*School of Mechanical and Materials Engineering and UCD Energy Institute,  
University College Dublin, Belfield, Dublin 4, Ireland*

<sup>b</sup>*Department of Geoscience and Remote Sensing,  
Delft University of Technology, 2628 CN, Delft, The Netherlands*

<sup>c</sup>*Urban Modelling Group, School of Civil Engineering,  
University College Dublin, Belfield, Dublin 4, Ireland*

<sup>d</sup>*E3D, RWTH Aachen, Aachen, Germany*

<sup>e</sup>*Mary Immaculate College, Limerick, Ireland*

<sup>f</sup>*New York University, New York, USA*

---

## Abstract

Current processes that create Building Energy Performance Simulation (BEPS) models are time consuming and costly, primarily due to the extensive manual inputs required for model population. In particular, generation of geometric inputs for existing building models requires significant manual intervention due to the absence, or outdated nature of available data or digital measurements. Additionally, solutions based on Building Information Modelling (BIM) also require high quality and precise geometrically-based models, which are not typically available for existing buildings. As such, this work introduces a semi-automated BEPS input solution for existing building exteriors that can be integrated with other related technologies (such as BIM or CityGML) and deployed across an entire building stock. Within the overarching approach, a novel sub-process automatically transforms a point cloud obtained from a terrestrial laser scanner into a representation of a building's exterior façade geometry as input data for a BEPS engine.

---

*Email addresses:* james.odonnell@ucd.ie (James O'Donnell),  
l.truong@tudelft.nl (Linh Truong-Hong), niamh.boyle.1@ucdconnect.ie (Niamh Boyle), edward.corry@mic.ul.ie (Edward Corry), cao@e3d.rwth-aachen.de (Jun Cao), debra.laefer@nyu.edu (Debra F. Laefer)

*Preprint submitted to Automation in Construction*

*August 8, 2019*

Semantic enrichment is performed manually. This novel solution extends two existing approaches: (1) an angle criterion in boundary detection and (2) a voxelisation representation to improve performance. The use of laser scanning data reduces temporal costs and improves input accuracy for BEPS model generation of existing buildings. The approach is tested herein on two example cases. Vertical and horizontal accuracies of 1% and 7% were generated, respectively, when compared against independently produced, measured drawings. The approach showed variation in accuracy of model generation, particularly for upper floors of the test case buildings. However, the energy impacts resulting from these variations represented less than 1% of the energy consumption for both cases.

*Keywords:* Light Detection And Ranging (LiDAR), Laser Scanning, City-Scale Modelling, Building Energy Performance Simulation (BEPS), Retrofit, Semi-Automated Façades Generation

---

## 1. Introduction

The advantages of creating and using Building Energy Performance Simulation (BEPS) models for existing buildings are well known. Such models can be used during design to predict energy usage, calibrated to reflect current building consumption, and employed to aid optimisation procedures [1]. However, there is a significant performance gap between predicted and actual performance for the majority of existing buildings [2, 3, 4] - implying limitations of existing models - which may be ascribable to discrepancies in their geometric representation. Other BEPS related factors include modelling assumptions, modeller errors, calculation errors within the programme and the absence of model updates that mirror changes to the building over its life cycle. Typically, BEPS models are associated with the design phase of the building life-cycle (BLC) and are not usually updated to reflect changes that occur to the building over time [5]. In cases where the model has been updated to reflect such changes in the physical building and its operations and subsequently calibrated, BEPS models have been shown to be instrumental in achieving greater operational efficiency [6]. Furthermore, as a decision making tool, BEPS models can compare alternatives during retrofit design scenarios [7]. Consequently, such tools are desperately needed as countries struggle to meet carbon emission and energy consumption targets within the context of the existing building stock.

22 For example, within Europe, authorities predict that 80% of the cur-  
23 rent building stock will still exist in 2050. Thus, scalable solutions must be  
24 developed to serve the extensive retrofitting market associated with these  
25 buildings [8]. BEPS tools can serve as an enabling mechanism for the im-  
26 proved operational performance of such buildings and groups of buildings [9].  
27 Unfortunately, the process of creating relevant models is complex, expensive,  
28 and time consuming and involves the manual input of a significant amount of  
29 data [10]. Automating the process of entering building geometry into BEPS  
30 tools could be a critical motivator to encourage building practitioners to use  
31 such tools throughout the BLCs of existing buildings.

32 Notably, there have been many recent advances in automated building  
33 model generation, particularly in BIM based solutions, whereby BIM geom-  
34 etry is traced over a point cloud captured by laser scanning, also known as  
35 Light Detection and Ranging (LiDAR). In BIM based solutions, the model  
36 is generated in BIM authoring tools such as Revit or ArchiCAD or through  
37 hybrid methods. Such hybrid methods tend to have significant manual input  
38 requirements [11, 12] and are, thus, not easily extendable to district-level or  
39 city-level investigations. Additionally, while the hybrid approaches have been  
40 used in an energy optimisation context, solutions using point clouds have not  
41 been used as a basis for automated geometric parameter input within the  
42 BEPS sphere, despite its widespread availability for building groups [13] and  
43 its potential impact in facilitating cost-effective BEPS models of individual  
44 buildings.

45 From a BEPS model development perspective, the key issue is the crea-  
46 tion of the BEPS geometry [14]. Automated and semi-automated solutions  
47 aim to ease the burden for BEPS modellers, but such approaches require  
48 precisely defined inputs in a BIM format such as IFC [15, 16, 17]. Thus,  
49 creating a BIM for an existing building, especially with the view to BEPS  
50 modelling is a challenging task. Given the nature and need for large-scale  
51 building retrofits and a parallel move towards interlinked digital models that  
52 capture and represent the built environment over time, proposed solutions  
53 must concentrate on efficient and cost-effective BEPS model development.  
54 Such a model must represent a building’s status and be updated with rela-  
55 tive ease to account for retrofit design alternatives, thereby, allowing for the  
56 quantification of the proposed impact of individual and combined retrofit  
57 measures, as well as changes in user behaviours. To date, leveraging LiDAR  
58 data for BEPS has not been considered feasible for energy simulation tools.  
59 Although Garwood et al. [18, 19] presented interesting advances and a large-

60 scale case study in the area of point cloud processing, their process requires  
61 manual intervention during the interpretation of the point cloud data. Since  
62 the fundamental inputs for BEPS tools are two-dimensional (2D) planes rep-  
63 resenting zone surfaces enclosed by a series of connected lines, BEPS tools are  
64 incapable of interpreting a point cloud associated with its attributes without  
65 post-processing. Traditional approaches use intermediary programmes, es-  
66 pecially those that are based on Computer Aided Drawing (CAD) programs.  
67 However, they require significant manual intervention to convert point clouds  
68 into the lines and planes required for BEPS inputs, and production difficulties  
69 may arise due to having to manage massive quantities of data points.

70 Several methods have been developed to automate the reconstruction of  
71 internal building components, e.g. walls, doors, ceilings and floors. For  
72 example, Budroni et al. proposed a plane-based sweep algorithm to detect  
73 the walls, ceilings and floors [20]. In this implementation, the vertical sweep  
74 initially extracted horizontal planes, and vertical walls were detected using  
75 a horizontal sweep. By using the advantages of a voxelisation model, Valero  
76 et al. decomposed a point cloud into a voxel space [21]. By examining the  
77 distribution of voxels in the horizontal plane, the floors and ceilings were  
78 contained a large number of voxels, and the point clouds within these voxels  
79 became inputs for the floors and ceilings. The remaining data points were  
80 projected onto a 2D horizontal plane to create a binary image. The walls  
81 were then identified by using a Hough Transform. An approach presented by  
82 Sanchez et. al. extracted point clouds of floors, ceilings and walls by using  
83 normal vectors of the points [22]. Then alpha shapes were used to fit the  
84 floors, ceilings and walls. In contrast, Shi et. al. combined a region-based  
85 segmentation and model-based segmentation to extract building surfaces [23].

86 In summary, the cost for reconstructing a 3D building model is still high.  
87 For example, when Garwood et. al. combined external and internal scan-  
88 ning to reconstruct building geometry and to determine the thickness of the  
89 building components (e.g. thickness of the walls and ceilings or floors), the  
90 process took several weeks to create a 3D geometry model using Leica Cy-  
91 clone software [19]. In response, this paper proposes a seamless, efficient, and  
92 robust process for generating geometrically accurate models for BEPS from  
93 terrestrial laser scanning data. Notably, the proposed method can work with  
94 multiple building shapes and components and can overcome missing data.

95 This paper addresses current research gaps that persist when using in-  
96 termediate data formats such as IFC or gbXML, as further transformation  
97 processes from these formats have limitations that result in data loss and er-

108 rors when applied at scale. IFC to BEPS tools are currently at the prototype  
109 stage only and require consistent, high quality inputs. They are, therefore,  
110 not sufficiently robust. As a result, such approaches are not yet ready for  
111 wide-scale deployment. Approaches that first map to gbXML prior to en-  
112 ergy modelling have a systematic limitation, as gbXML uses the centre-line  
113 for representation of geometry. In the context of energy simulation in build-  
114 ings, this centre-line convention typically results in discrepancies in calculated  
115 surface areas and volumes, which significantly exceed standard engineering  
116 tolerances and cause over estimations of building energy consumption, as  
117 defined by Bazjanac et. al. [24].

118 Consequently, the aim of this work is to develop a new methodology for  
119 extracting the exterior geometry of a building appropriate for BEPS mod-  
120 elling. This is to be achieved through the use of a terrestrial laser scanner  
121 (TLS) and an automatic, seamless, scalable, and robust method for recon-  
122 structing 3D building models without any third party software or manual  
123 intervention. This representation is subsequently transformed using a short,  
124 semi-automatic process into a format that is directly usable for building en-  
125 ergy performance simulation. In doing so, the proposed solution overcomes  
126 many limitations such as (1) incorrect geometric representations in gbXML  
127 and (2) extremely precise geometric definitions in the IFC format when pro-  
128 cessing IFC for energy modelling conversions. In this case, the transformation  
129 is for BEPS modelling of existing buildings. The semi-automated nature of  
130 the approach represents an important step towards deploying BEPS mod-  
131 elling across groups of buildings, an important consideration as cities move  
132 towards interlinked digital representations of all building assets. The remain-  
133 der of the paper is organised into five sections.

Section 2 describes the state-of-the-art in this area, while Section 3 out-  
lines the methodology behind the semi-automated process for building façade  
generation. The novel method to transform the resulting data into the format  
required for building simulation purposes is then illustrated (Section 4). The  
validation methods for the models are discussed, and a demonstration of the  
process is given (Section 5). Finally, in Section 6, conclusions, limitations,  
and possible future work in this area are addressed.

## 131 2. Related Work

132 Western societies have a pressing need for scalable, building-specific so-  
133 lutions that address a largely energy inefficient building stock [8]. Recent

134 developments in the area of building innovation for energy use reduction  
135 have primarily focused on identifying retrofitting measures, while dismissing  
136 the use of BEPS tools because of the cost, time, and effort needed to de-  
137 velop and calibrate such models. Additionally, BEPS tools typically gener-  
138 ate entity-averaged outputs, as opposed to identifying localised discrepancies  
139 [25] (i.e. average wall heat flux ( $\text{W}/\text{m}^2$ ), or identifying wall segments with  
140 poor insulation levels). However, BEPS can be an enormously useful tool  
141 when evaluating a range of retrofit alternatives. Since the goal of the paper  
142 is to develop an automatic process to create 3D building models for BEPS  
143 from LiDAR data, the related work section is restricted to the creation of  
144 3D building thermal profiles and building energy modelling. Input data for  
145 those purposes can be thermographic imagery and/or laser scanning data.  
146 For other aspects relating to building energy modelling, readers are referred  
147 elsewhere (e.g. Cho et al. [10]).

148

### 149 **Three-dimensional building thermal profiles**

150 Increasingly, efforts to visualise building energy at a city scale are being  
151 undertaken. Two notable projects of significant size include the Energy Atlas  
152 Berlin [26] and SEMANCO [27]. Both projects predict a rudimentary annual  
153 energy usage for each building within the study area. The Berlin project in-  
154 cludes approximately 500,000 buildings [26]. The geometric building models  
155 were created from a combination of aerial laser scanning (ALS) data and  
156 2D footprints, that were then textured with photographs of the building  
157 façade. In contrast, the SEMANCO project proposed a platform support-  
158 ing improved energy analysis based on existing data, which was applied to  
159 three urban areas with a combined population exceeding 150,000 people [27].  
160 In this project, a set of tools were also developed to automatically create  
161 3D maps from aerial photography and a digital earth model (DEM) or dig-  
162 ital terrain model (DTM), with the corresponding energy usage integrated  
163 for visualisation. In related work, López et al. [28] presented a complete  
164 methodology for generating thermographic 3D point clouds of urban areas  
165 by using a thermographic camera to acquire thermal data and mobile laser  
166 scanning to collect building topography. Similarly, a combination of TLS  
167 data and aerial ortho-photography was used to manually create 3D build-  
168 ing models with level of detail (LoD) 2 for computational fluid dynamics  
169 (CFD) analysis to estimate temperatures in urban environments [29], but  
170 the method proved time consuming in both data acquisition and building  
171 model generation.

172 In an effort to explore detailed energy consumption of the building, Lagüela  
173 et al. [30] mapped thermal images onto the point cloud of the building to  
174 measure energy efficiency directly. Similarly, González-Aguilera et al. [31]  
175 textured thermographic images onto a 3D point cloud of a building, which  
176 was generated from matching thermographic images. Lagüela et. al.. [32]  
177 textured as-built models with RGB and thermographic images to diagnose  
178 and analyse building energy usage. The proposed method created the build-  
179 ing model as a set of intersection lines between the building surfaces, where  
180 the doors and windows were not included. Focusing on interiors, Borrmann  
181 et al. [33] used a mobile robot to integrate a thermal camera and laser scan-  
182 ning sensor for automatic data acquisition and generated a full thermal model  
183 of a building's interior. Additionally, Cho and Wang [34] used a TLS and  
184 a thermal camera to generate 3D point cloud models for building envelopes  
185 with the corresponding temperature values at the individual point level.

186 Significant research initiatives have developed efficient methods to create  
187 accurate 3D building energy profiles, but these methods do not explicitly  
188 exploit building geometry. As such, the models for mapping thermal infor-  
189 mation therein cannot be used directly in energy tools. Work in that area is  
190 described in the next section.

191

## 192 **Building Energy Modelling**

193 A geometric building model is a crucial part of BEPS. With recent de-  
194 velopments in point cloud acquisition and processing, 3D geometric building  
195 models have the potential to support building energy modelling. However,  
196 in practice, 2D geometric information is still primarily used for energy mod-  
197 elling. For example, Moran et al. [35] applied the Passive House Planning  
198 Package tool to assess energy usage and CO<sub>2</sub> emissions in historic buildings  
199 in the city of Bath. For that effort, manually collected, 2D geometric data  
200 of building components were used. Similarly, to evaluate energy retrofiting  
201 results, Morelli et al. [36] created building envelopes of existing structures  
202 by employing the software Be10, where the geometric building model was  
203 derived from building planning documents.

204 Three-dimensional building models are increasingly being used to improve  
205 the accuracy of energy simulation. For example, Ham and Goparvar-Fard [37]  
206 evaluated predicted building energy performance derived from a combination  
207 of CFD and EnergyPlus software against actual measurements from digital  
208 and thermal imagery. Thermal image information was mapped onto building  
209 models created from a large number of digital images, which allowed users to



210 visualise and compare actual measurements and simulated results in a com-  
211 mon 3D environment. Several automatic algorithms have been developed  
212 to create either exterior or interior 3D building models, but certain limi-  
213 tations persist: (1) primarily applicable to relatively simple buildings [38];  
214 (2) require a priori knowledge [39]; and/or (3) give relatively low geometric  
215 accuracy [40]. Amongst the methods for exterior building model reconstruc-  
216 tion, Zolanvari and Laefer [41] recently proposed a slicing method to divide  
217 the building façade into the number of independence horizontal and vertical  
218 strips. The points of the strip were then compressed into line segments, and  
219 the end points of the line segments were known as boundary points. The  
220 method provides relatively high levels of accuracy for the boundary points  
221 and single façades but does not create automatically complete building mod-  
222 els. Similarly, Li et al. detected the corners of openings based on the gradient  
223 of the number of points within the sliding window search along both hori-  
224 zontal and vertical directions [42]. Although the method can work properly  
225 for a case of partial missing data, it is limited for façades with rectilinear and  
226 repetitive openings.

227 Moreover, with a recent demand for BIM and indoor navigation, recent  
228 methods mostly focus on generating indoor building models but accurate  
229 detection and generation of openings (doors and windows) is still difficult for  
230 older and complex structures [43]. For example, in reconstructing openings  
231 from interior point clouds, Adan and Huber used the Hough transform to  
232 detect boundary lines based on boundary points of openings extracted from  
233 an binary image of a wall [44]. This work reported an average absolute  
234 error of 5.39cm for window dimensions with a standard deviation of 5.70cm  
235 when compared to the ground truth. Díaz-Vilariño et al. generated building  
236 models from TLS data that had door and window errors typically ranging  
237 from 2.8% to 6.5%, with a maximum error of 34.3% [40]. Wang and Cho used  
238 data points on the edges of the building and its windows for BEPS tools [45]  
239 . However, the generated building geometry had a relatively low accuracy  
240 with average errors of around 16.9% and 12.5% for the window widths and  
241 lengths, respectively.

242 Jung et al. used boundary tracing to extract boundary points of in-  
243 terior walls and openings from binary images [46]. Subsequently, a con-  
244 strained least-squares adjustment approach generated boundary lines from  
245 these boundary points – the accuracy of the interior building components  
246 depends on grid size and threshold distances. The study also calculated a  
247 root mean square error (RMSE) between a 3D wireframe model’s vertices

248 and a ground truth derived from total station measurement of about 4.8cm.  
249 Tamke et al. used supervised learning techniques to detect and classify open-  
250 ings from a point cloud of interior building walls [47]. The method can detect  
251 openings with a success rate 91.2% for doors and 72.8% for the windows but  
252 with 39.5% classification error. The extracted doors and windows averaged  
253 9.8% smaller than ground truth in a terms of area. Ochmann et al. presented  
254 a method that can detect openings with an accuracy about 85.2% [48]. As  
255 an alternative, Quintana et al. decomposed a point cloud into voxels, which  
256 are classified as occupied, occluded and opening voxels [49] and used Otsu’s  
257 global histogram threshold technique and the Canny edge detector to iden-  
258 tify openings from colour and depth images, respectively. An accuracy of  
259 98.3% in terms of opening areas was achieved, but only for rectangular open-  
260 ings. Similarly, Jung et al. converted the point cloud of wall segments into  
261 a binary image to detect hollow areas potentially representing openings and  
262 boundaries [43]. The shape and size of the hollow areas were used to remove  
263 incorrect openings. The algorithm successfully generated all walls and de-  
264 tected all openings but was sensitive to grid cell size. The study reported  
265 root mean square errors between reference points and reconstructed wall ver-  
266 tices of 8.9cm and 7.4cm but detailed geometric accuracy of openings was  
267 not been reported.

268 By deploying a spatial representation, Staats [50] used a voxelisation  
269 model to detect doors for indoor navigation from handheld indoor laser scan-  
270 ning data. The doors were detected with a high fluctuation of voxels in both  
271 vertical and horizontal directions. The authors determined that the method  
272 can detect about 84.2% actual doors. Li et al. decomposed a point cloud of  
273 a story into cells and the line fitting was used to create the wall edges from a  
274 binary image of the wall [51]. The maximum errors varied from  $4.29 \pm 0.53cm$   
275 to  $45.74 \pm 5.52cm$  in terms of distance between vertices, or from  $-0.86 m^2$   
276 to  $4.51 m^2$  in terms of area. In the worst case, the algorithm detected about  
277 82% of the walls and doors in the model.

278 In other related work, Tran et al. proposed a shape grammar to gener-  
279 ate 3D indoor building models through a simple primitive and interactive  
280 grammar rules [52]. Although the method can reconstruct building elements  
281 for various data sets through a visual evaluation, the method still requires  
282 manual adjustment for the locations of histogram peaks and correction of  
283 the classification labels. Shi et al. combined region-based segmentation for  
284 wall with openings and predefined opening dimensions were used to elimi-  
285 nate false positives [23]. Although that method can detect the number of

286 openings, geometric accuracy was not been reported. Moreover, in an at-  
287 tempt to explore the backpack scanning data for indoor modelling, Wang et  
288 al. used an  $\alpha$ -shape based method to extract the boundary points of each  
289 façade, and a k-mean clustering method was used to extract potential lines  
290 of doors and windows from internal lines of the wall [53]. Like many others,  
291 this algorithm is applicable only for rectangular openings. Finally, to over-  
292 come limited availability of laser scanning data for buildings, Neuhausen and  
293 König [54] detected windows from images through two main steps. First, a  
294 machine learning method extracted the windows but the detection accuracy  
295 was quite low, at about 69%. To improve the detection rate in the second  
296 step, the authors applied an image-based edge detection technique to extract  
297 the windows' boundary lines. Next, a knowledge base using window patterns  
298 in the façade and detected windows in a previous step were used to detect  
299 missing windows. This implementation improve the detected rate to 95.2%.  
300 However, the accuracy of the window size may be limited, because the au-  
301 thors defined the boundary lines of the window from the average of a set of  
302 edges detected from regions surrounding the window.

303 In current practice, building energy usage estimation usually differs from  
304 the actual energy performance [45]. This can occur for reasons that include  
305 comparisons using as-designed building models (as opposed to as-built build-  
306 ing models) or building models with a low level of detail (LoD), thus resulting  
307 in significant geometric discrepancies between the input model and the actual  
308 operational building. For example, when an LoD2 building model is used,  
309 openings (i.e. doors and windows) are not explicitly modelled. When a LoD3  
310 model with the major external features such as doors, windows, and a correct  
311 roof shape is used, it must be transformed for use in BEPS software; see [55]  
312 for a more detailed set of definitions for various LoDs. However, achieving  
313 this at scale has not been realisable to date.

314 Although significant complementary information can be added to geomet-  
315 ric models of buildings, the initial creation of a building geometry is most  
316 commonly done through a manual process that is both time consuming and  
317 expensive. Recent advances in laser scanning and photogrammetry based  
318 techniques for building reconstruction offer more opportunities for develop-  
319 ing as-built building models for the purposes of BEPS. Nonetheless, a robust,  
320 efficient, automatic workflow for accurate 3D building model reconstruction  
321 has remained a significant challenge; this is particularly true in the case of a  
322 detailed BEPS model requiring the geometry of the building including a cross  
323 section and coordinate information for floors, walls, ceilings, roofs, columns,

324 and doors.

### 325 **3. Method**

326 The goal of the proposed method is to automatically process point cloud  
327 data for building façades into a format usable by all BEPS tools with minimal  
328 manual intervention; the method was validated by testing on one BEPS  
329 engine (EnergyPlus). The process also includes validation of simulation input  
330 and a mechanism to check geometric configurations through visualisation of  
331 DXF files, which are generated by the target BEPS tool. The proposed  
332 method has two key sub-processes (Figure 1): (1) point cloud data capture  
333 and processing to create 3D geometric building models from terrestrial laser  
334 scanning data (Section 3.1) and (2) BEPS creation (Section 4.1).

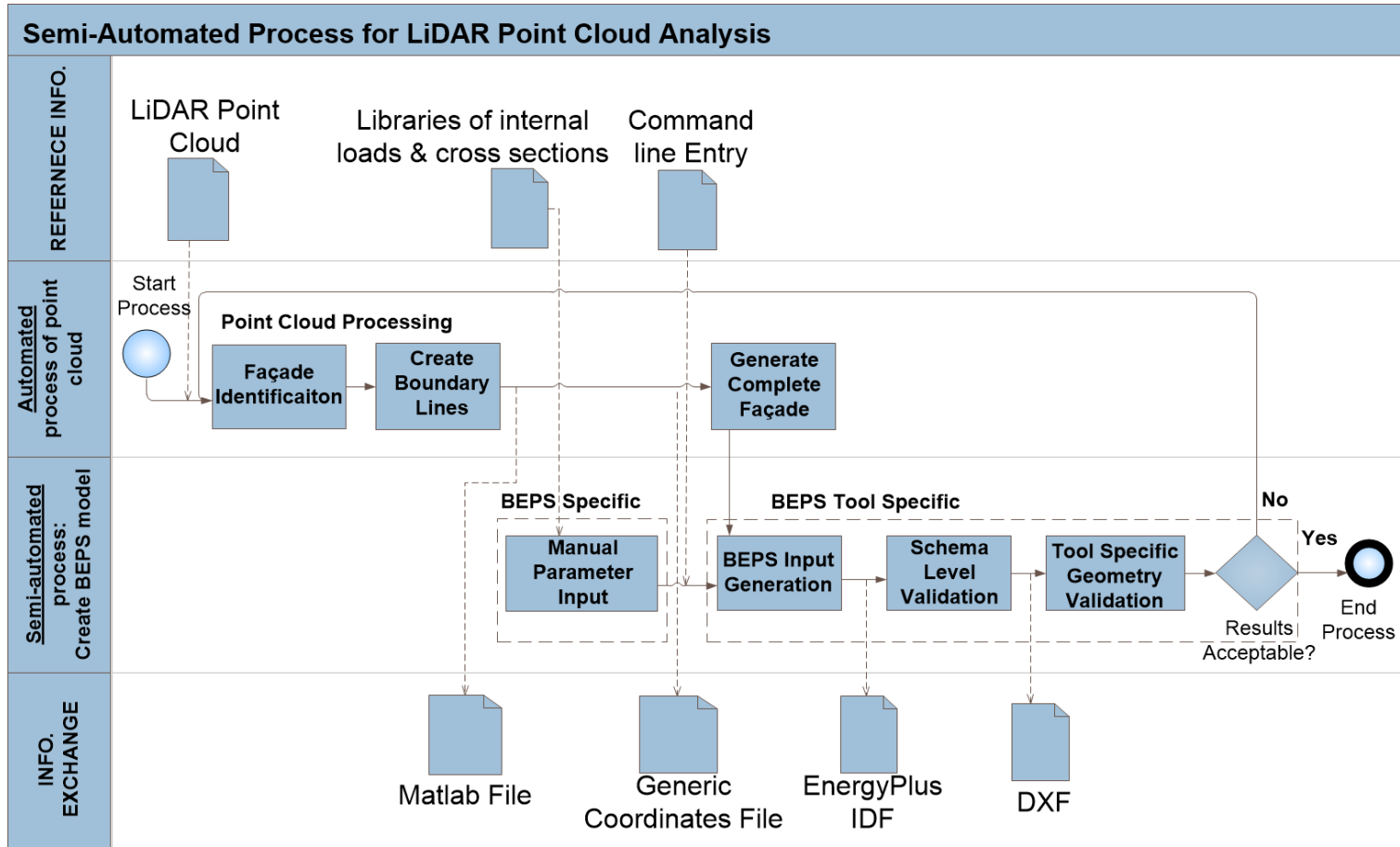


Figure 1: Process Diagram representing a semi-automated workflow that converts point cloud information into a format compatible with BEPS tools

335 3.1. Point cloud processing

336 Processing the point cloud consists of three main steps, as illustrated in  
 337 Figure 2: (1) extraction of a portion of a point cloud capturing the façade  
 338 of the building from the scanned data points; (2) creation of boundary lines  
 339 of the façade and its openings (i.e. doors and windows), which are based on  
 340 points on their boundaries, and (3) creation of a 3D geometric model of the  
 341 building façades. This work presumes that building features reside within  
 342 vertical walls and that doors and windows are primarily glass-plated or are  
 343 recessed. For the purpose of this work, architectural details were intentionally  
 344 ignored.

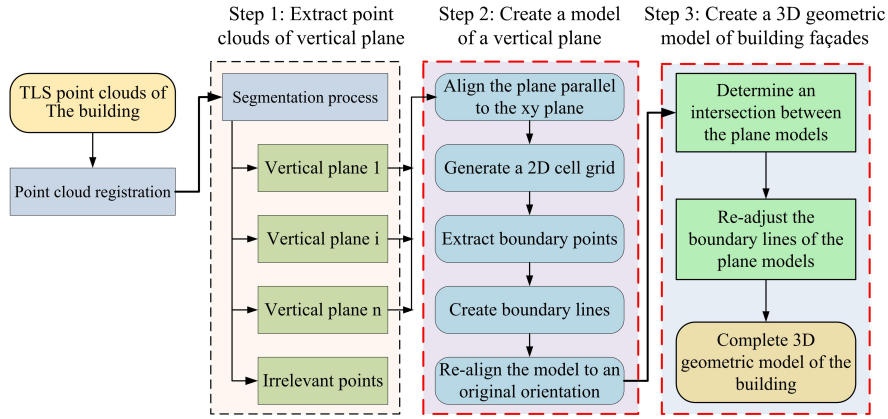


Figure 2: Proposed method for façade reconstruction using laser scanning data

345 The workflow begins with the registration of multiple point clouds of the  
 346 building, acquired from different point of views due to footpath limitations  
 347 and obstacles. The registration process can be done through using artificial  
 348 targets or objects' features (e.g. edges or corners of façade planes). In prac-  
 349 tice, the registration was done by using the scanner's proprietary software,  
 350 for example, Leica Cyclone for the Leica scanners or RealWorkSurvey for  
 351 Trimble scanners [56], which took less than 5 minutes to register 3 to 5 point  
 352 clouds. Next, the point cloud of the building with x-, y-, and z- coordinates  
 353 was exported as input data for the proposed method.

354 The resulting registration included a large amount of redundant points in-  
 355 cluding those of interior components, terrain, vehicles, and adjacent façades.  
 356 Since the 3D building model generally involves multiple surfaces and compli-  
 357 cated shapes, reconstructing building models from the full set of data points

358 remains a large challenge. Step 1 uses a segmentation process to partition  
 359 the 3D scene data points into multiple surfaces to create an input for Step  
 360 2. Although many segmentation methods can extract the point cloud of  
 361 a building façade (e.g. [57, 58, 59]) significant user input or judgement is  
 362 commonly needed to tune input parameters or filter spurious segments. In  
 363 this work, a voxel-based region growing method [59] is employed to extract  
 364 the data points on the same planar surface. This automatic approach relies  
 365 heavily upon an octree indexing structure to separate the points into two  
 366 groups: (1) building exterior and (2) other (e.g. internal building compo-  
 367 nents, vehicles, or noise), which can be eliminated. For more details of the  
 368 segmentation method, refer to Vo et al. [59]. Next, the point cloud of each  
 369 façade or vertical plane is sequentially processed to identify boundary lines  
 370 of a building and its features.

371 Since each vertical exterior surface of the building consists of a set of  
 372 points,  $\mathbf{P} = \{p_i, i = (1, \dots, n)\} \in \mathbb{R}^3$ , boundary lines for its entirety and its  
 373 features (doors and windows) are created from the data points  $\mathbf{P}$  (Step 2). In  
 374 this work, each exterior wall is assumed to be a vertical, largely flat surface,  
 375  $\mathbf{S}$ . Next, the data points of the surface ( $\mathbf{P}$ ) are projected onto a plane parallel  
 376 to the xy plane of the global coordinate system (GCS) by mapping principal  
 377 directions of the fitting plane of the façade onto the unit vectors of the GCS,  
 378 which are given in Equation 1. The principal directions or eigenvectors of  
 379 each wall are determined by employing a principal component analysis (PCA)  
 380 [60].

$$\begin{Bmatrix} x \\ y \\ z \end{Bmatrix} = R_z(\beta_3)R_y(\beta_2)R_x(\beta_1) \begin{Bmatrix} X \\ Y \\ Z \end{Bmatrix} \quad (1)$$

381 Herein, the data points of each wall are described as x-, y-, and z-  
 382 coordinates in the GCS, where x and y axes are now, respectively, the hori-  
 383 zontal and vertical directions of the wall, while the z coordinates of all points  
 384 are the same (Figure 3a). The 3D model of each wall can be generated by  
 385 extruding its 2D model in the x-y plane along the z-axis, with a predefined  
 386 wall thickness.

387 In order to generate boundary lines of the façade and its openings (e.g.  
 388 doors and windows), a 2D cell grid is employed to represent the decomposi-  
 389 tion of an entire façade into non-overlapping 2D regions, commonly referred  
 390 to as cells (step 2.1). An initial bounding box of all projected points  $\mathbf{P}$  can  
 391 be defined by two pairs of coordinate values  $(x_{min}, y_{min})$  and  $(x_{max}, y_{max})$ .

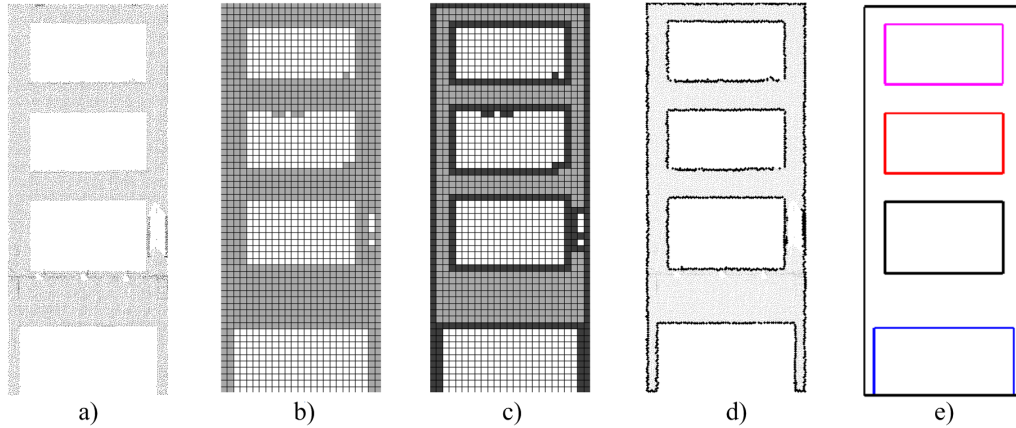


Figure 3: a) Input data b) Initial 2D cell grid c) Full cells containing candidate points d) Boundary points e) Boundary lines of the wall

392 Subsequently, a cell grid divides a bounded, 2D region into a set of regular  
 393 cells by grids along the x- and y-axes in a Cartesian coordinate system. Each  
 394 cell is described by an index, a geometry, and a property. The index is de-  
 395 fined as  $c(i, j)$ , where  $i \in [1; N_x]$ ,  $j \in [1; N_y]$ , and  $N_x$  and  $N_y$  are defined in  
 396 Equations (2) and (3). The geometry is stored as a centre  $[x_{cen}, y_{cen}]$  and a  
 397 cell size, while the property is either "full" or "empty" (described by 1 and 0,  
 398 respectively). A cell is full, if it contains at least one data point. Otherwise,  
 399 it is empty (Figure 3b).

400 In this method, the empty cells within the building wall are assumed to  
 401 describe the inside of doors and windows or holes due to missing data. An  
 402 opening is only detected, if one or more empty cells appear inside a candidate  
 403 area for an opening. Thus, the predefined cell size plays an important role  
 404 within the method proposed by this paper. If the cell size is too large, no  
 405 empty cell may be available within the area of the door or window. On  
 406 the other hand, if the cell size is too small, particularly if it is less than the  
 407 sampling step of the data point, a number of empty cells may appear over the  
 408 area of the building wall, which in turn lead to over-detection of openings.  
 409 Truong-Hong and Laefer [61] proved that a predefined cell size of 0.2m is  
 410 an appropriate value to generate at least one empty cell within doors and  
 411 windows corresponding to a minimum opening size of 0.4m, as established  
 412 from a survey of urban window sizes [62]. With a predefined cell size of 0.2m,  
 413 the number of cells along the horizontal and vertical directions are given in



414 Equations 2 and 3.

$$N_x = \frac{x_{max} - x_{min}}{cell\_size} + 1 \quad (2)$$

$$N_y = \frac{y_{max} - y_{min}}{cell\_size} + 1 \quad (3)$$

415 Next, the process extracts points on boundaries of the façade and its  
416 openings. This is referred to as the boundary point extraction step. Although  
417 several other methods are potentially available (e.g half-disk criterion [63],  
418 triangulation mesh [64], multiple criteria [65]), in this work, an angle criterion  
419 [66] is employed to extract the boundary points from a set of candidate points.  
420 However, unlike previous work with an angle criterion (e.g. [66]), where all  
421 data points must be checked as to whether they are boundary points or not,  
422 the method herein only examines possible points (called candidate points),  
423 which are the data points in the vicinity of the boundaries of the wall and  
424 its openings. In the cell representation of the façade or wall (Figure 3b),  
425 the full cells containing the candidate boundary points of the doors/windows  
426 are connected to an empty cell group appearing as a hole inside the façade,  
427 while those of the façade boundary connect to the empty cell group along  
428 the outside of the façade and/or attach to the minimum bounding box of the  
429 data set. Extraction of the full cells possessing the candidate points is shown  
430 in (Figure 3c).

431 A candidate boundary point is a boundary point, if the maximum angle  
432 between two consecutive neighbour points exceeds an angle threshold by  
433  $90^\circ$ ; for full details on the selection of the angle threshold and the process  
434 of extracting boundary points see Truong-Hong et al. [66]. Additionally,  
435 the selection of neighbour points differs from that proposed by Truong-Hong  
436 et al. [66], where a k-d tree was required for neighbour point searching.  
437 In this work, the process starts with a full cell ( $c(i, j)$ ) containing a given  
438 point. Other full cells ( $c(k, l)$ ) connected to  $c(i, j)$  are then extracted. The  
439 neighbour points of the given point are the rest of the data points within  $c(i,$   
440  $j)$  and all of the points within  $c(k, l)$ .

441 Notably, due to occlusions, unrealistic holes may appear on the wall.  
442 In order to eliminate those holes, the height ( $H_0$ ) and width ( $L_0$ ) of each  
443 hole is computed from its boundary points and compared to dimensions of  
444 common openings in the building. A hole is considered a real opening, if its  
445 height and length satisfy the conditions expressed in Equation 4, where the  
446 minimum opening size is 0.4m [64, 38], and its height-to-width ratio varies

447 from 0.25 to 5.0 [62]. Figure 3d highlights the process of distinguishing real  
 448 from unrealistic openings and infilling the unrealistic openings.

$$f(H_0, L_0, \frac{H_0}{L_0}) = \begin{cases} H_0 \geq 0.4; L_0 \geq 0.4; 0.25 \leq H_0/L_0 \leq 5 : \textit{Opening} \\ \textit{Otherwise} : \textit{Non - opening} \end{cases} \quad (4)$$

449 Next, a boundary line for a building component is created from the bound-  
 450 ary points (Figure 4a). In the method proposed herein, boundaries of the  
 451 building wall and associated openings are assumed to consist of a set of ver-  
 452 tical, horizontal, and/or inclined lines. A region growing method is then  
 453 adopted to separate the boundary points of the wall and its openings, in  
 454 which the data points of each group are distributed on the same pattern  
 455 (either vertical, horizontal, or inclined) (Figure 4b). As part of this, the tan-  
 456 gent vector of each boundary point is computed from its k-nearest neighbour  
 457 (kNN) points using PCA, for which a neighbourhood of 10 kNN points is rec-  
 458 ommended. The initial seeding point is selected from the boundary points;  
 459 this point is chosen based on the smallest deviation angle between its tangent  
 460 vector and a unit vector ( $n_y = [0,1,0]$ ). If the angles between the seeding  
 461 point and boundary points in the kNN point(s) are smaller than an angle  
 462 threshold (recommended as  $5^\circ$  based on empirical trials), the kNN points are  
 463 added iteratively into the seeding point group. This process is applied, until  
 464 all boundary points are checked.

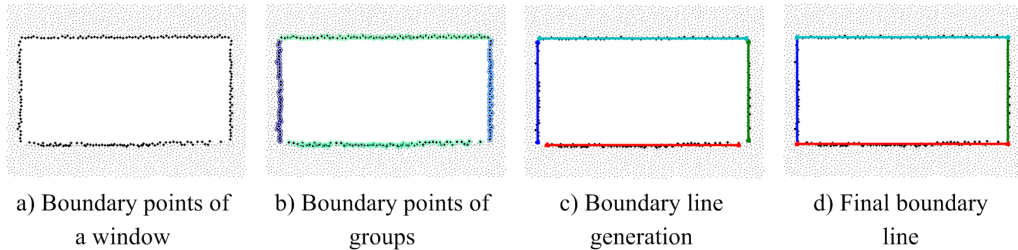


Figure 4: Illustration of boundary line generation for a building feature

465 Subsequently, each resulting group is classified as vertical, horizontal,  
 466 and/or inclined for the purpose of creating the boundary lines of the build-  
 467 ing features. A tangent vector of the group is computed from the group's  
 468 boundary points. The classification of the group's pattern is determined  
 469 based on the deviation angle between the tangent vector of the group and

470 the unit vector. If the deviation is less than the angle threshold, for exam-  
471 ple  $5^\circ$ , the unit vector is  $(n_y = [0,1,0])$  for vertical and is  $(n_x = [1,0,0])$  for  
472 horizontal. Otherwise, the group’s pattern is classified as inclined. Notably,  
473 the group is only considered for further processing, if the length of its pat-  
474 tern is greater than or equal to half of the minimum opening size (0.4m)  
475 [61]. Then, boundary lines are generated from the boundary points of each  
476 group ( $L = \{p_i = (x_i, y_i, z_i) | 1 \leq i \leq k\}$ ) and the group’s pattern classification.  
477 Vertical and horizontal patterns are expressed in Equations 5 and 6, respec-  
478 tively, while a least mean squares fitting [67] is applied to the inclined pattern  
479 (Figure 4c). Next, the boundary lines of each feature are adjusted to ensure  
480 continuity by extending or trimming the boundary lines at their intersection  
481 points (Figure 4d). The final boundary lines of the wall and its openings are  
482 shown back in Figure 3e. Geometric information for those boundary lines is  
483 in the plane parallel to the xy plane within the GCS, which is not the original  
484 orientation of the surface. Equation 1 is used to re-map the boundary lines  
485 into the original plane of the vertical surface or the façade.

486 For vertical patterns:

$$x_0 = \frac{\sum_{i=1}^k x_i}{k}; y_{min} = \min(y_i); y_{max} = \max(y_i) \quad (5)$$

487 For horizontal patterns:

$$y_0 = \frac{\sum_{i=1}^k y_i}{k}; x_{min} = \min(x_i); x_{max} = \max(x_i) \quad (6)$$

488 In reality, a building often contains multiple vertical surfaces or façades.  
489 After extracting the point cloud of each vertical wall (Step 1), the bound-  
490 ary lines of the wall and its openings are separately reconstructed using the  
491 procedure in Step 2. For example, with a point cloud of the building in Fig-  
492 ure 5a, the segmentation process automatically extracted the point clouds of  
493 2 vertical walls. The proposed method was applied to reconstruct boundary  
494 lines for each vertical wall shown in Figure 5c. However, there is a gap be-  
495 tween two adjacent vertical walls because of (1) missing edge points during  
496 data acquisition [68], (2) the fact that segmentation methods do not allow  
497 edge points to belong to multiple segments (or walls), and (3) a procedure in  
498 which boundary line reconstruction takes the data points along boundaries  
499 of building components, which leads and shrinks them to the bounding box  
500 of the vertical wall (Figure 5c). Therefore, to reconstruct a 3D water-tight

501 building model for BEPS, a new boundary line between two adjacent vertical  
 502 surfaces must be created, instead of having two boundary lines (one for each  
 503 vertical surface) (Figure 5b and c). The process starts by determining the  
 504 parametric equation of the surface in the form of the centre and normal of  
 505 the surface. From a set of vertices  $P_i$  ( $i = 1, \dots, N$ , where  $N$  is the number  
 506 of vertices) of the boundary lines, the surface centre is a centroid of  $P_i$ , while  
 507 the surface normal is the eigenvector corresponding the smallest eigenvalue  
 508 computed from a covariance matrix of  $P_i$ . Next, a pair of adjacent vertical  
 509 walls (or façades),  $S_i$  and  $S_j$ , of the building can be determined based on the  
 510 Euclidean distance  $d(P_i, P'_i)$  horizontally, which is calculated from  $x$  and  $y$   
 511 coordinates of  $P_i$  and  $P'_i$ , where  $P_i$  and  $P'_i$  are respectively the boundary  
 512 vertices of  $S_i$  and  $S_j$  (Figure 5c and d) [67]. In this implementation, if any  
 513  $d(P_i, P'_i)$  is less than 1.4 times of the cell size, a pair of surfaces are judged  
 514 to be adjoining vertical walls [69]. An intersection line is computed using  
 515 the surface equations, in this example  $S_1(q_1, n_1)$  and  $S_2(q_2, n_2)$ , where  $(q_1,$   
 516  $n_1)$  and  $(q_2, n_2)$  are the centres and normal vectors. The result is shown in  
 517 Figure 5d. Subsequently, the vertical boundary lines of  $S_1$  and  $S_2$  closest to  
 518 the intersection line are replaced by the intersection line. Finally, the set  
 519 of boundary lines of each surface is extended or trimmed to ensure a set of  
 520 closed boundary lines for each vertical surface. Through this procedure the  
 521 final reconstructed building model can be achieved as shown in Figure 5e.  
 522 In addition, vertical gaps ranging from millimeters to centimeters may be  
 523 present at the top of the adjacent façades, which arise due to errors of data  
 524 segmentation or boundary line reconstruction (Figure 5e). In order to over-  
 525 come this issue, a possible solution is to retrieve boundary points used to  
 526 generate boundary lines at the top of the façades. A new surface ( $S_{atop}$ ) can  
 527 be generated through these boundary points, and the new boundary lines on  
 528 the top of the façade is an intersection line between the façade surface and  
 529  $S_{atop}$ . This step will be fully implemented in future work.

530 At this stage, the 3D exterior building model comprises multiple polylines  
 531 to represent boundaries of the building and its openings (doors and windows).  
 532 The vertices for each surface are determined using two iterations: (1) the first  
 533 stores vertices of the exterior polylines that represent the boundary of each  
 534 surface and (2) the second iteration stores vertices of the interior polylines  
 535 describing the boundary of the windows or doors belonging to the surface. If  
 536 the surface has no opening, the second iteration fails to return any vertices.  
 537 Both iterations have an ID that can be easily used to retrieve the geometric  
 538 information of the surface for further processing.

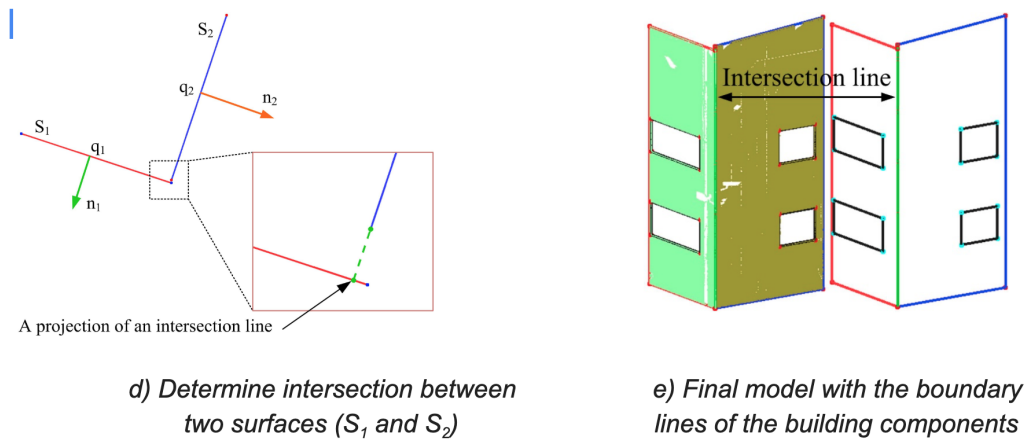
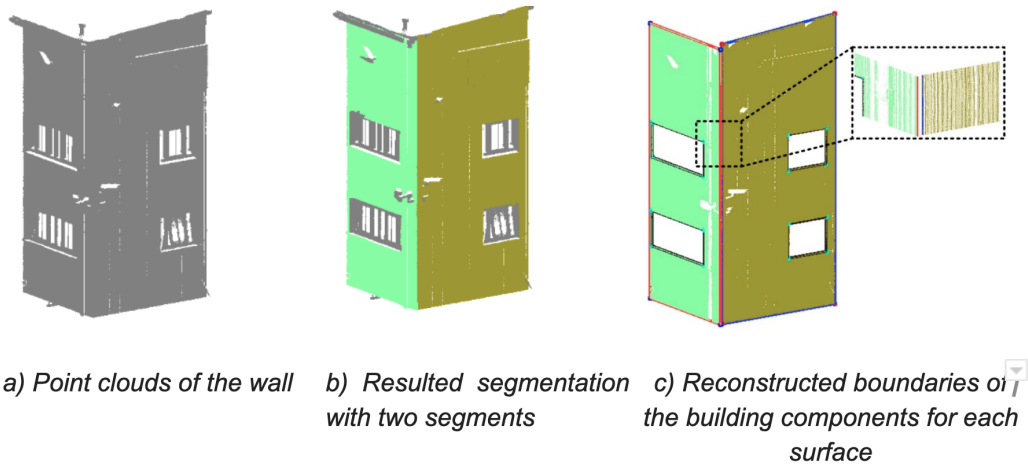


Figure 5: Process to overcome gaps between vertical surfaces of a building's exterior wall

539 Additional information including spatial and semantic information about  
540 the building and environment variables is required in order to simulate build-  
541 ing energy use based on the exterior geometry of the building.

542 The next step (Section 4) transforms the processed point cloud and manu-  
543 ally inserted data into the syntax required by the target BEPS engine, in  
544 this case, EnergyPlus.

#### 545 4. BEPS Creation and Model Validation

546 This section describes the process of creating and validating a BEPS  
547 model. In line with the process illustrated in Figure 1, a number of se-  
548 quential steps including defining a number of concise manual inputs that  
549 enable automatic conversion of the processed building geometry into a for-  
550 mat suitable for a valid simulation run (Section 4.1); generating neutral and  
551 tool-specific BEPS files (Section 4.2); validating at the schema level (Section  
552 4.3) and validating in the BEPS tools and post-processing (Section 4.4).

553 Most of the commonly available BEPS engines are based on one-dimensional  
554 heat transfer. In the context of building façades, the information required by  
555 these comparable BEPS tools is identical or almost identical. Notable consid-  
556 erations are as follows: (1) the order of points when defining surfaces and (2)  
557 the definition of zone-surface, surface-subsurface and surface to cross-section  
558 relationships [70]. The key parameters are:

- 559 • Surface name
- 560 • Parent surface name (relevant for doors and windows);
- 561 • Location of vertices using a standard coordinate system and;
- 562 • References to the cross-section type and the surface thermal properties.

563 Other information such as surface normals, view factors, and surface areas  
564 can be calculated from the information provided. An important difference  
565 between BEPS tools is the syntax through which the information is rep-  
566 resented. Therefore, the conversion process would be almost identical for  
567 similar BEPS tools but with some minor syntax related variations. HVAC  
568 system and component representations are beyond the scope of this paper,  
569 if HVAC information was in a neutral file then very different conversion pro-  
570 cesses would be required for each BEPS tool. Furthermore the transformation  
571 process that uses the neutral file format must be consistent with the process  
572 presented by [16, 71].

573 *4.1. Manual Parameter Input*

574 Following the generation of a 3D geometric model for a given building,  
575 additional geometric and semantic information must be added to create input  
576 data for the BEPS tool. Geometric parameters include floor elevation and  
577 thickness of each floor slab and wall. While, these parameters could be  
578 automatically obtained by integrating laser scanning data from the exterior  
579 and interior of the building, such steps are out of the scope of this paper.

580 Semantic information includes the primary function of each floor (e.g.  
581 retail or office), the age of the building or year of the most recent major  
582 retrofit, and the materials of the windows, doors, walls, floors, and roof.  
583 Similarly, environmental information including usage profiles and equipment  
584 power densities must also be manually entered or can be selected from a  
585 template such as in Lagüela et al. [72]. The combination of this additional  
586 information with the processed point cloud is then used to create the wall,  
587 window, door, roof, and floor entities, as well as to determine the location of  
588 the windows and doors.

589 U-values are referenced by building element instances (wall, window or  
590 door) where each building element references a cross-section definition; for  
591 example Figure 6 contains a reference to a cross-section called “SinglePane-  
592 GlassWindow”). Each cross-section comprises a number of material layers  
593 that are stored in a defined order. The material properties for each material  
594 layer are available from public and proprietary sources or could be extracted  
595 from other scanning approaches such as that presented in Wang et al. [73].  
596 U-values are calculated at run-time from the material layer properties of each  
597 cross-section.

598 Thermal zones or volumes of the buildings that are at the same environ-  
599 mental conditions are the fundamental building blocks of traditional BEPS  
600 simulations and must also be defined. The process starts with  $\mathbf{Z} = \{z_i, i =$   
601  $(0, \dots, N)\}$ , the series of floor elevations, where  $z_0$  and  $z_N$  are respectively  
602 the elevation of the ground and roof level. This implies that the number of  
603 zones (or storeys) within the building is  $N$ , and the lower and upper bounds  
604 of the zone  $i$  are  $z_i$  and  $z'_i = z_{i+1} - s_i$ , where  $s_i$  is the thickness of the floor  
605 slab  $i$ -th. Next, exterior surfaces of each zone are the exterior surfaces of  
606 the building vertical walls bounded by the lower and upper bounds of the  
607 zone, while the interior surfaces can be created by offsetting the exterior sur-  
608 face with the wall thickness. Thus, the geometric information for the zone  
609 involves interior surfaces and additional floor and ceiling or roof surfaces, re-  
610 spectively and openings (doors and windows) associated with the zone. The

611 openings belonging to the Zone can be determined by comparing the vertices  
 612 of the openings generated in a previous step to the lower and upper bounds  
 613 of the zone. The opening is classified as a door, if any of its vertices connect  
 614 to the ground level [39], otherwise, it is a window. Finally, for each zone,  
 615 geometric and semantic information associated with environmental parameters  
 616 are stored in the neutral file according to the specification syntax required.  
 617 At this point the BEPS data are in a neutral representation, the syntax of  
 618 which must be adjusted to account for a specific BEPS tool (Section 4.2).

#### 619 4.2. Neutral and Tool Specific BEPS File Generation

620 The file is created based on the outputs of the automated point cloud  
 621 mapping and the manually added data. Figure 6 illustrates the representation  
 622 of an example window in the standard ORACLE format for polygons,  
 623 the neutral file format and the EnergyPlus file format. A one-to-one mapping  
 624 of points and other properties is the key step in the conversion to the neutral  
 625 file format. Please note that while the neutral file format closely aligns with  
 626 the EnergyPlus file format, it is not identical.

Point Cloud Data Format	Neutral File Format	Comment	EnergyPlus IDF Format
INSERT INTO Surface_With_Window VALUES( 10, 'polygon_with_hole', SDO_GEOMETRY( 2003, -- two-dimensional polygon NULL, NULL, SDO_ELEM_INFO_ARRAY(1,1003,1, 19,2003,1), -- polygon with hole SDO_ORDINATE_ARRAY(2.0, 14.0, 14.5, 2.5, 2.0, 4.2, 7.2, 7.5, 4.5, 4.2) ) );	FenestrationSurface, Window 1, Window, SinglePaneGlassWindow, Wall 1, Outside, AutoCalculate, , 1, 1, 4, 4.0, 0.0, 2.0, 7.0., 0.0, 2.0, 7.0., 0.0, 5.0, 4.0, 0.0, 5.0,	!- Object Type !- Object Type !- Opening Type !- Cross-section Name !- Parent Object Name !- Ouside Boundary Condition !- View Factor !- Shading Control Name !- Frame and Divider Name !- Multiplier !- Number of Vertices !- Vertex 1 Coordinates !- Vertex 2 Coordinates !- Vertex 3 Coordinates !- Vertex 4 Coordinates	FenestrationSurface:Detailed Window 1, Window, SinglePaneGlassWindow, Wall 1, Outside, AutoCalculate, , 1, 1, 4, 4.0, 0.0, 2.0, 7.0., 0.0, 2.0, 7.0., 0.0, 5.0, 4.0, 0.0, 5.0,

**Legend**

Data from Point Cloud Process	
Manually Added Data	

Figure 6: A window example for the three stages of data in the overall semi-automated process: point cloud format, the neutral file format and the EnergyPlus IDF format

627 The neutral file is of .txt format and does not adhere to the input format  
 628 of any given BEPS tool. This approach follows the conventions adopted by  
 629 seminal work in this area [16, 71].

630 The neutral file can be converted to a specific BEPS tool input format  
 631 using a script or conversion tool. The design of this format allows for a one-to-  
 632 one mapping of property instances between the neutral file (example provided  
 633 in Figure 6) and the BEPS input file. The neutral file stores geometric  
 634 information only and is not executable in any BEPS engine, the mandatory  
 635 properties include:



- 636     • Surface name;
- 637     • Surface Type (wall, floor, ceiling or roof)
- 638     • Parent surface name (relevant for doors and windows);
- 639     • Outside boundary condition for the surface (set to outside for all façade  
640       surfaces) and;
- 641     • location of each vertex using a standard coordinate system;

642     This information is complemented by the manually inserted parameter  
643     values that include:

- 644     • Cross section name
- 645     • Zone name for parent surfaces
- 646     • Outside boundary condition
- 647     • Outside boundary condition object
- 648     • Sun exposure (optional)
- 649     • Wind exposure (optional)

#### 650    4.3. Schema Level Validation

651     Model validation is then performed at two levels. The first is a routine  
652     validation against the target data model schema, while the second is within  
653     the modelling tool for verification of model suitability for compilation. These  
654     steps are discussed in detail below.

655     Validation of the BEPS inputs is specific to the targeted BEPS tool, for  
656     example EnergyPlus. The first rudimentary check is a comparison of the  
657     generated input file against the EnergyPlus schema file, called the Input  
658     Data Dictionary (IDD). This check is performed in a basic input tool called  
659     the IDF Editor, an interface for the EnergyPlus Input Data Format (IDF).

660     The schema level validation is a check that the input file is valid for a  
661     specific BEPS run, for example the contents of an XML file should adhere to  
662     the rules defined in a corresponding BEPS XSD schema. There are numer-  
663     ous XML or JSON tools available for this type of check, and such a check  
664     should be performed easily outside of a given simulation engine. Many of the

665 established BEPS tools, such as EnergyPlus and DOE-2, are based on legacy  
666 system architectures that predate modern day best practice approaches for  
667 data management and do not have a formal schema. As a result, EnergyPlus  
668 does not provide this type of schema level validation prior to execution of a  
669 model. However, Simergy, an interface to EnergyPlus does. EnergyPlus is in  
670 the process of moving to a JSON schema and input files ([74]). Each BEPS  
671 tool should have its own rigorously defined schema.

#### 672 *4.4. Validation in BEPS Tool and post-processing*

673 EnergyPlus is one of the most popular BEPS tools that engineers, archi-  
674 tects, and researchers use to model energy and water usage in buildings and  
675 includes the most popular features and capabilities of the software packages  
676 BLAST and DOE-2.1E. As a result of the legacy code-base, key compilation  
677 and validation checks are performed during run-time, rather than beforehand.  
678 Various errors may then be generated, for example:

- 679 • Order of vertices when defining a surface;
- 680 • Surface normals pointing outward from the zone, as opposed to inward;
- 681 • Zones not enclosed;
- 682 • View factors;
- 683 • Incomplete data defined for a simulation run.

684 After the files are successfully uploaded to EnergyPlus, the requested  
685 output is a DXF file that is generated by the energy simulation tool for a  
686 final visualisation check. This technique has been applied in other relevant  
687 works in this area [16, 15]. The DXF file also describes floor and ceiling  
688 positions within the building.

## 689 **5. Test case evaluation**

### 690 *5.1. Experimental tests*

691 The objectives of the experiment were to evaluate the accuracy of the  
692 models generated by the proposed method and to determine to what extent  
693 such discrepancies impact downstream energy performance predictions. This  
694 was achieved through a comparison of (1) geometric measurements and (2)

695 the annual energy consumption of BEPS models based on terrestrial laser  
 696 scanning (TLS) data and independently measured CAD drawings. The pro-  
 697 posed semi-automated process described in Sections 3 and 4 was applied to  
 698 two buildings in Dublin, Ireland: No. 25 Westmoreland St. and No. 6  
 699 D’Olier St. These two buildings represent geometrically complex cases with  
 700 different opening sizes and shapes. Both buildings have corresponding CAD  
 701 drawings, which were used as the benchmark models when validating the  
 702 building façade models. Building suitability was based on the time-period of  
 703 construction. Each building has a different configuration of floors, windows,  
 704 and doors (Figure 7a and Figure 8a). Actual geometric information for each  
 705 building was based on a traditional survey and derived from drawings sub-  
 706 mitted to the Planning and Property Development Civic Offices of Dublin  
 707 City Council (Table 2 and 3). Specific dimensions included length, height,  
 708 and depth of the building, the dimensions of the building’s openings, thick-  
 709 ness of floor slabs and walls, and the floor elevation. The façade for No. 25  
 710 Westmoreland St. contains 5 floors, with 4 small doors (Door type I) and  
 711 1 large door (Door type II) on the bottom floor, 6 windows (Window type  
 712 I) on the first floor, 5 small windows (Window type II) and 1 large window  
 713 (Window type III) on the second floor, and 6 windows (Window type IV and  
 714 V) on the fourth and fifth floors. Similarly, No. 6 D’Olier St. contains 5  
 715 floors, with a door (Door type I) and 3 large windows (Window type I and  
 716 II) on the bottom floor, and 3 windows (Window type III, IV and V) on each  
 717 subsequent floor.

Table 1: Size of the data sets for the two buildings

Building	Sampling data set		
	S20	S50	S75
No. 25 Westmoreland st.	353,848	71,155	35,468
No. 6 D’Olier st.	177,480	39,259	20,089

718 Point cloud data for these buildings were collected by a Trimble GS200  
 719 terrestrial laser scanner. Each building façade was scanned from different  
 720 views to avoid omissions due to occlusions, and the data points were regis-  
 721 tered within RealWorkSurvey (RWS) V6.3. The source data set were mapped  
 722 to the target based on pre-selected reference points, which are sharp features  
 723 (e.g. a corner of the surface or window) although several methods could be

724 used, for example surface matching algorithms [75]. The point cloud for the  
725 building of interest had to be manually separated from adjacent buildings  
726 within RWS V6.3, a current limitation of automatic extraction [76]. Next,  
727 the voxel-based region growing approach was employed to segment the data  
728 points of the building of interest using the approach and input parameters  
729 proposed by Vo et al. [59]. The results of segmentation allowed for elimi-  
730 nation of irrelevant data points (e.g. internal objects such as furniture and  
731 ceilings). Thus, remaining data points describe vertical surfaces of the build-  
732 ing and serve as input data for the proposed method, as defined in Section  
733 3.1. For each building, three different sampling steps involving 20mm, 50mm  
734 and 75mm, were used to evaluate the influence of the sampling step on the  
735 geometric models. The TLS data of these buildings are shown in Table 1.  
736 Additionally, the selected terraced buildings are in an urban area, where it  
737 is extremely difficult to acquire data pertaining to side and back walls [39].  
738 Therefore, in the process of 3D building generation based on TLS data, two  
739 assumptions were proposed: (1) the back wall is parallel to the street façade  
740 but has no openings and can be generated by offsetting the the façade (not  
741 including openings) by the building depth, and (2) the side walls can be au-  
742 tomatically generated by sweeping the side edges of the façade to the back  
743 wall [39]. Results of the building façade models from the proposed method  
744 are illustrated in Figure 7b, Figure 8b, and Table 2 and 3. Notably, since  
745 dimensions of each reconstructed opening in each storey of the façade differ,  
746 average dimensions of the reconstructed openings are shown in Tables 2 and  
747 3.

748 The BEPS model for each building was automatically created by combin-  
749 ing geometric building data generated from the proposed method in this  
750 paper with semantic information and environmental parameters. The geom-  
751 etry of the building was generated in a previous step, while the semantic  
752 information, such as the year of construction or the last major renovation  
753 for a given building was manually collected. The cross section types were  
754 assumed to be single course walls with interior plaster and single pane win-  
755 dows with wooden frames. Material layer properties of each cross-section  
756 were entered accordingly. The rudimentary modelling approach isolated the  
757 façade under investigation by representing these walls, windows and doors  
758 in details but all other surfaces as adiabatic, thus, focusing on the energy  
759 related impacts of the single façade alone. All zones used a constant temper-  
760 ature set point of 21°C for heating without a provision for cooling. Finally,  
761 Dublin, Ireland was set as the location, and both models used a simulation

762 period of one year, for which publicly available climate data were used in the  
763 weather file.

764

765



Figure 7: (a) Westmoreland Street Façades and (b) Resulting building reconstruction from the proposed method

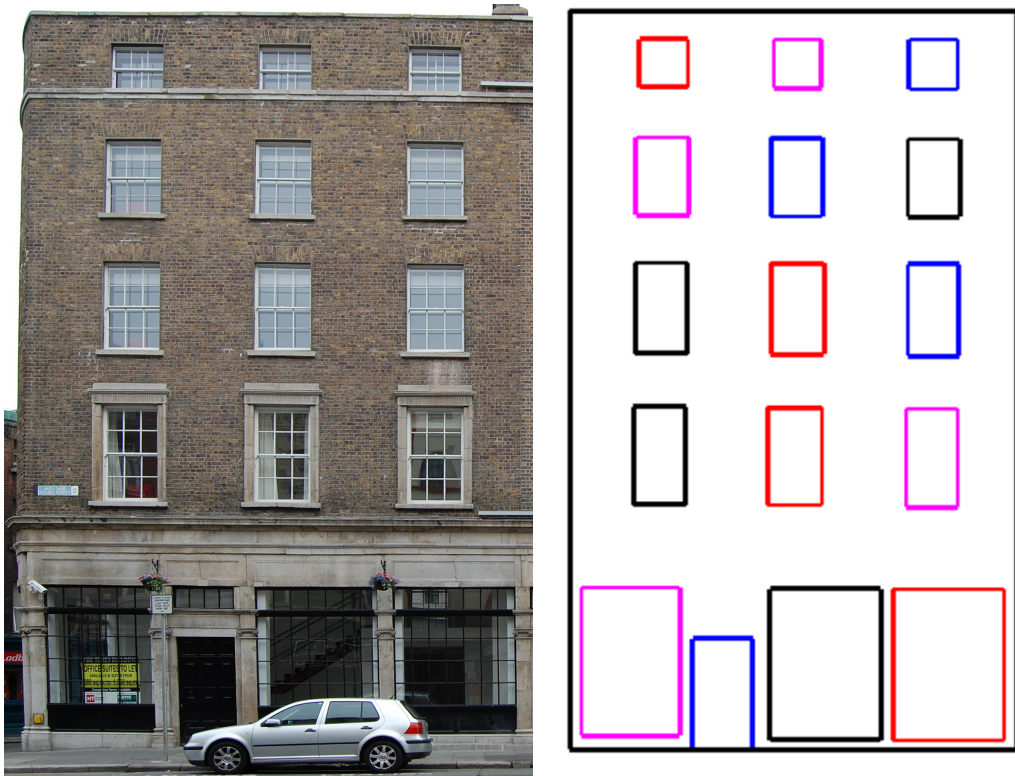


Figure 8: (a) D'Olier street façade and (b) Resulting building reconstruction from the proposed method, with evidence of occlusion

Table 2: Geometric information for No. 25 Westmoreland St.<sup>(\*)</sup> denotes a manual BEPS entry for building models reconstructed from TLS data

		CAD	S20	S50	S75
Façade	Length (m)	19.36	19.31	19.27	19.24
	Height (m)	17.00	16.90	16.88	16.87
	Opening area (m <sup>2</sup> )	96.17	96.71	98.02	99.18
	Depth (m)	11.03*			
	Wall thickness (m)	0.60*			
	Slab thickness (m)	0.296*			
	Number of storeys	5			
S1	Height: Flr.-Flr. (m)	4.25	4.25	4.25	4.25
	Door I (WxH) (m)	2.00x3.60	2.00x3.56	2.02x3.56	2.03x3.56
	Door II (WxH) (m)	4.90x3.60	4.92x3.56	4.93x3.56	4.95x3.56
	Tot. opening area (m <sup>2</sup> )	46.44	45.97	46.27	46.51
	Tot. floor area (m <sup>2</sup> )	213.56	213.00	212.53	212.24
	Tot. zone volume (m <sup>3</sup> )	844.42	842.21	840.35	839.20
S2	Height: Flr.-Flr. (m)	3.61	3.61	3.61	3.61
	Window I (WxH) (m)	1.25x2.06	1.25x2.04	1.27x2.05	1.28x2.06
	Tot. opening area (m <sup>2</sup> )	15.42	15.28	15.61	15.78
	Tot. floor area (m <sup>2</sup> )	213.56	213.00	212.53	212.24
	Tot. zone volume (m <sup>3</sup> )	710.94	709.08	707.52	706.55
S3	Height: Flr.-Flr. (m)	3.10	3.10	3.10	3.10
	Window II (WxH) (m)	1.25x1.65	1.25x1.66	1.26x1.67	1.27x1.69
	Window III (WxH) (m)	4.20x1.65	4.17x1.72	4.18x1.74	4.21x1.75
	Tot. opening area (m <sup>2</sup> )	15.17	15.45	15.71	15.95
	Tot. floor area (m <sup>2</sup> )	213.56	213.00	212.53	212.24
	Tot. zone volume (m <sup>3</sup> )	594.55	593.00	591.69	590.88
S4	Height: Flr.-Flr. (m)	3.03	3.03	3.03	3.03
	Window IV (WxH) (m)	1.25x1.65	1.26x1.63	1.27x1.65	1.28x1.67
	Tot. opening area (m <sup>2</sup> )	12.36	12.32	12.56	12.83
	Tot. floor area (m <sup>2</sup> )	213.56	213.00	212.53	212.24
	Tot. zone volume (m <sup>3</sup> )	583.87	582.35	581.06	580.27
S5	Height: Flr.-Flr. (m)	3.02	2.92	2.90	2.89
	Window V (WxH) (m)	1.25x0.90	1.26x1.03	1.27x1.03	1.24x1.10
	Tot. opening area (m <sup>2</sup> )	6.78	7.69	7.87	8.11
	Tot. floor area (m <sup>2</sup> )	213.56	213.00	212.53	212.24
	Tot. zone volume (m <sup>3</sup> )	580.67	558.40	552.81	549.45

Table 3: Geometric information for No. 6 D’Olier St. (\*) denotes a manual BEPS entry for building models reconstructed from TLS data

		CAD	S20	S50	S75
Façade	Length (m)	10.50	10.53	10.52	10.14
	Height (m)	17.46	17.43	17.42	17.42
	Opening area (m <sup>2</sup> )	52.76	53.53	53.84	54.02
	Depth (m)	10.85(*)			
	Wall thickness (m)	0.60(*)			
	Slab thickness (m)	0.296(*)			
	Number of storeys	5	5	5	5
S1	Height: Flr.-Flr. (m)	5.29	5.29	5.29	5.29
	Door (WxH) (m)	1.30x2.65	1.39x2.62	1.40x2.62	1.42x2.62
	Window I (WxH) (m)	2.58x3.50	2.61x3.54	2.61x3.55	2.62x3.56
	Window II (WxH) (m)	2.26x3.50	2.31x3.49	2.33x3.51	2.33x3.50
	Tot. opening area (m <sup>2</sup> )	25.97	26.51	26.67	26.79
	Tot. floor area (m <sup>2</sup> )	113.92	114.27	212.53	212.24
	Tot. zone volume (m <sup>3</sup> )	568.94	570.67	569.97	569.68
S2	Height: Flr.-Flr. (m)	3.50	3.50	3.50	3.50
	Window III (WxH) (m)	1.20x2.34	1.25x2.29	1.25x2.30	1.24x2.31
	Tot. opening area (m <sup>2</sup> )	8.43	8.55	8.59	8.61
	Tot. floor area (m <sup>2</sup> )	113.92	114.27	114.13	114.07
S3	Height: Flr.-Flr. (m)	3.50	3.50	3.50	3.50
	Window IV (WxH) (m)	1.20x2.15	1.22x2.15	1.23x2.15	1.23x2.15
	Tot. opening area (m <sup>2</sup> )	7.74	7.89	7.92	7.92
	Tot. floor area (m <sup>2</sup> )	113.92	114.27	365.67	114.07
S4	Height: Flr.-Flr. (m)	3.00	3.00	3.00	3.00
	Window V (WxH) (m)	1.20x1.85	1.22x1.83	1.23x1.84	1.23x1.84
	Tot. opening area (m <sup>2</sup> )	6.66	6.70	6.75	6.78
	Tot. floor area (m <sup>2</sup> )	113.92	114.27	308.61	114.07
S5	Height: Flr.-Flr. (m)	2.17	2.14	2.13	2.13
	Window VI (WxH) (m)	1.20x1.10	1.14x1.14	1.14x1.15	1.14x1.15
	Tot. opening area (m <sup>2</sup> )	3.96	3.88	3.91	3.92
	Tot. floor area (m <sup>2</sup> )	113.92	114.27	114.13	114.07
	Tot. zone volume (m <sup>3</sup> )	568.94	210.26	209.76	209.07



766 *5.2. Results*

767 The proposed method successfully generated 3D building models com-  
 768 patible with BEPS tools with only minimal manual intervention required.  
 769 The models of the two buildings derived from the S50 data set are shown  
 770 in Figure 9, while a summary of building geometries is presented in Table 2  
 771 and 3. Reconstructed building façade models with height and width values  
 772 generally differed by under 1%, in terms of a relative error when compared to  
 773 equivalent values from the reference data, a maximum absolute difference of  
 774 130 mm was found in the height of No. 25 Westmoreland St. Moreover, the  
 775 proposed method also produced a building façade with an approximately 3%  
 776 larger opening area than those in the reference data. The largest difference  
 777 in terms of an opening area is 3.01 m<sup>2</sup> in No. 25 Westmoreland St. from  
 778 the S75 data set. Similarly, dimensions of the reconstructed openings were  
 779 overestimated by an maximum absolute average 57.2 mm [standard devia-  
 780 tion (std) = 57.6 mm] for the height of No. 25 Westmoreland St.’s openings,  
 781 and 46.9 mm (std = 28.9 mm) for the width of No. 6 D’Olier St.’s open-  
 782 ings. Considering the discrepancy of openings’ dimensions for each zone, the  
 783 largest of which was found in zone 5 (top of the building). This is the max-  
 784 imum absolute difference of the window’s height, and is 191mm for No. 25  
 785 Westmoreland St based on the S75 dataset. This in turn translates to an  
 786 absolute difference of 1.33m<sup>2</sup> in terms of area. However, for other zones, in  
 787 both buildings, differences in the opening area were mostly less than 0.5m<sup>2</sup>.  
 788 Finally, when considering the difference of the building models derived from  
 789 CAD drawings and TLS data in term of a volume, the reconstructed building  
 790 models differ around 1.4% (No. 25 Westmoreland st - CAD vs. S75) and  
 791 3.6% (No. 6 D’Olier st. - CAD vs. S75). Note that this comparison is based  
 792 on height, length and depth of the building assumed as a block.

$$\begin{aligned}
 Relative_{DifferenceEnergy} = & -0.0354 + 1.8386 * Difference_{WallArea} + \\
 & 1.0172 * Difference_{OpeningArea}
 \end{aligned}
 \tag{7}$$

793 Results of annual energy consumption of the buildings based on CAD  
 794 and reconstructed models from TLS data are shown in Table 4. For No. 25  
 795 Westmoreland St., annual energy consumption from the CAD-based build-  
 796 ing was 89,142 kWh, which was greater than those from all generated model  
 797 results within 1% for this surface of this value. A similar observation was  
 798 found in No. 6 D’Olier St. The measured energy consumption based the

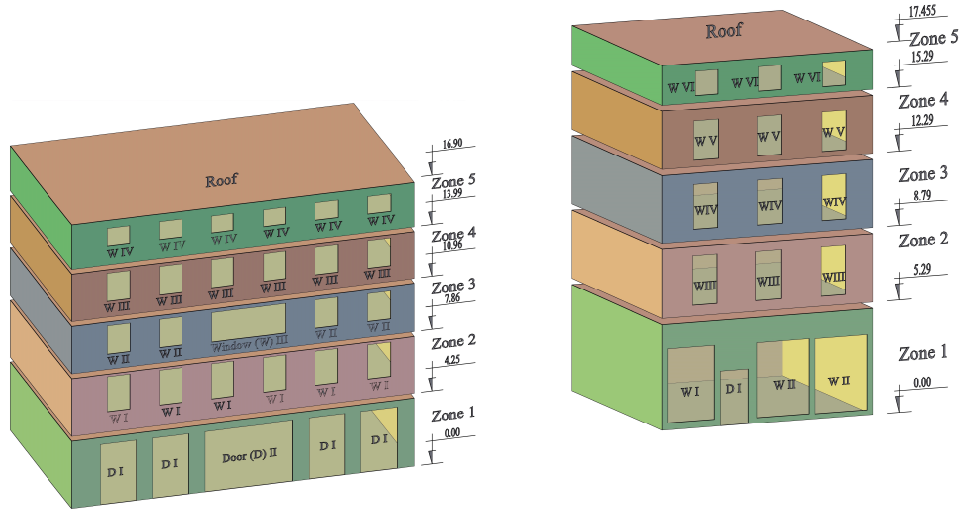


Figure 9: Illustration of building models for BEPS input (a) 25 Westmoreland st. and (b) 6 D'Olier st.

799 CAD model was 51,649 kWh, which is less than 1% smaller than those of all  
 800 three generated models. This error is acceptable given that these are sim-  
 801 plistic, indicative models, and in such cases, a model is considered calibrated  
 802 if measured energy consumption values are within 10% of BEPS predictions  
 803 on a monthly basis. The proposed semi-automated process could contribute  
 804 inputs to a detailed model that could also include detailed HVAC and oc-  
 805 cupancy descriptions. In such cases, far more stringent calibration criteria  
 806 would apply, which are beyond the scope of this paper.

807

808

809 Multi-variate linear regression was employed to explore the influence of  
 810 geometric discrepancy on annual energy consumption. The goal of this work  
 811 was to identify the relationship between the absolute difference in the building  
 812 geometries (i.e. wall and opening area) and the relative difference of annual  
 813 energy consumption (Table 5), where values from the CAD-based models  
 814 were considered as the reference values. The analysis represented this re-  
 815 lationship as in Equation 7 with  $R^2 = 0.93$ , as shown in Figure 10. This

Table 4: Annual building heating consumption (kWh)

Input data	CAD	S20	S50	S75	
No. 25 Westmoreland st.					
Heating	Zone 1	20,966	20,886	20,861	20,847
	Zone 2	19,005	18,941	18,944	18,941
	Zone 3	16,800	16,786	16,783	16,791
	Zone 4	16,427	16,386	16,380	16,391
	Zone 5	15,944	15,505	15,389	15,333
	<b>Total</b>	<b>89,142</b>	<b>88,504</b>	<b>88,357</b>	<b>88,303</b>
No. 6 D'Olier st.					
Heating	Zone 1	16,086	16,219	16,225	16,230
	Zone 2	10,111	10,155	10,150	10,147
	Zone 3	10,261	10,308	10,297	10,294
	Zone 4	8,900	8,930	8,927	8,927
	Zone 5	6,291	6,211	6,200	6,183
	<b>Total</b>	<b>51,649</b>	<b>51,823</b>	<b>51,799</b>	<b>51,781</b>

816 implies that the differences in wall and opening areas significantly influenced  
 817 the change of the annual energy consumption.

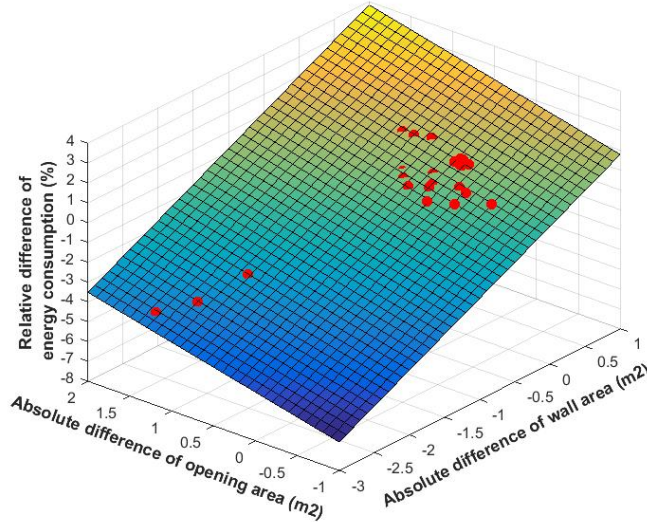


Figure 10: Relationship between building geometry and energy consumptions

Table 5: Absolute difference of geometry and relative difference of energy consumption

		No. 25 Westmoreland st.			No. 6 D’Olier st.		
		CAD vs. S20	CAD vs. S50	CAD vs. S75	CAD vs. S20	CAD vs. S50	CAD vs. S75
Wall area (m <sup>2</sup> )	Zone 1	-0.20	-0.37	-0.47	0.16	0.09	0.07
	Zone 2	-0.17	-0.31	-0.40	0.10	0.06	0.05
	Zone 3	-0.14	-0.26	-0.33	0.10	0.06	0.05
	Zone 4	-0.14	-0.25	-0.33	0.09	0.05	0.04
	Zone 5	-2.02	-2.53	-2.83	-0.24	-0.29	-0.35
Openings’ area (m <sup>2</sup> )	Zone 1	-0.47	-0.17	0.07	0.54	0.70	0.82
	Zone 2	-0.14	0.19	0.36	0.12	0.16	0.18
	Zone 3	0.28	0.54	0.78	0.15	0.18	0.18
	Zone 4	-0.04	0.20	0.47	0.04	0.09	0.12
	Zone 5	0.91	1.09	1.33	-0.08	-0.05	-0.04
Heating (%)	Zone 1	-0.38	-0.50	-0.57	0.83	0.86	0.90
	Zone 2	-0.34	-0.32	-0.34	0.44	0.38	0.36
	Zone 3	-0.08	-0.10	-0.05	0.46	0.35	0.32
	Zone 4	-0.25	-0.29	-0.22	0.34	0.31	0.31
	Zone 5	-2.75	-3.48	-3.83	-1.28	-1.46	-1.72

818 *5.3. Discussion*

819 This paper introduces a semi-automated, seamless, scalable, and robust  
820 method for reconstructing façades of 3D building models without require-  
821 ments for any third party software or a priori information. The proposed  
822 method is suitable for generating building models with features comprising  
823 linear boundaries; it cannot yet account for building components with non-  
824 linear (i.e. curve or circle) boundaries. Such functionality would require the  
825 introduction of additional algorithms or unsupervised learning techniques to  
826 classify component boundaries as linear and non-linear, with an accompany-  
827 ing fitting procedure to determine the boundary line of best fit based on the  
828 root mean square error of the fitting.

829 The proposed method was successful in the construction of 3D building  
830 models for two building façades from different sampling steps. Relative errors  
831 of the façades’ and openings’ dimensions are less than 1% and 3%, respec-  
832 tively, while the maximum average relative errors of opening areas are 6.4%  
833 for a data set of S75 from 25 Westmoreland St. and and 2.6% for 6 D’Olier  
834 St. This implies that the quality of the building models derived from the pro-

835 posed method is better than a previous work done by Díaz-Vilariño et. al.  
836 [40], which generated the openings with an average relative error of 11.7%.  
837 Moreover, although the sampling step is up to 75 mm (Table 1), the RMSEs  
838 of the façade dimensions and its openings are respectively 125.1 mm and 61.5  
839 mm for 25 Westmoreland st., and 27.3 mm and 46.1 mm for 6 D’Olier St.  
840 (Figure 11a & b). Those errors are generally less than the sampling step,  
841 which is consistent with the conclusions of Tang et al. [68]. In such cases,  
842 edge losses due to spatial discontinuities of a point cloud arise when the laser  
843 beam hits the edge of solid object and this can be up to several centimetres.  
844 Moreover, it also noted that the proposed method gave errors of the same or-  
845 der when compared to previous research: an average error for window size of  
846 5.39cm (std = 5.70cm) [44], an RMSE of the walls’ vertices about 4.8cm [46]  
847 and 7.4cm [43], a maximum distance error for the walls’ vertices in a range  
848 from  $4.29 \pm 0.53cm$  to  $45.74 \pm 5.52cm$ . Moreover, when considering an error  
849 in terms of an area, results from the proposed method are also comparable  
850 with a work of Tamke et al. [47] with an error about 9.8% or Quintana et  
851 al. [49] with an error of 1.7% regarding to detected openings.

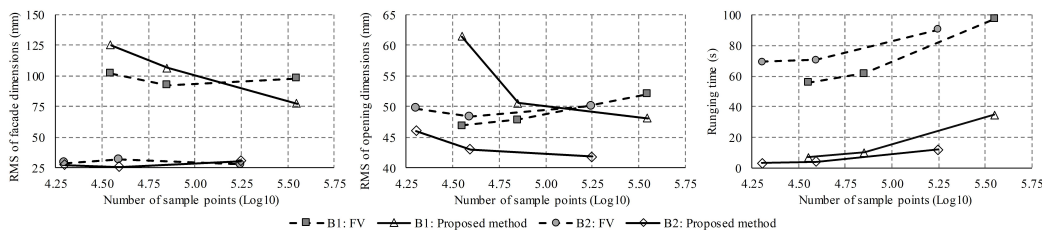


Figure 11: Comparing performance of the proposed method vs. the façade method developed by [61]: a) RMSE of façade’s dimensions, b) RMSE of openings’ dimensions, c) Running time

852 In addition, performance of the proposed method in terms of quality  
853 of the building models and execution time was compared to that of the  
854 façade voxel (FV) method developed by Truong-Hong and Laefer [61], an  
855 automatic method for 3D building reconstruction. Both algorithms were  
856 implemented in Matlab 2016a environment and run on a HP EliteBook 2570p  
857 with Intel (R) Core i7-3520M, CPU @2.9GHz, 16Gb RAM, OS Window 10.  
858 The geometric building models from the algorithms were compared to the  
859 CAD models to identify geometric discrepancies. Results showed that the  
860 proposed method can generate the building models with the same accuracy  
861 level to the building models from FV method. However, the proposed method

862 reconstructed successfully 25 Westmoreland St. - with 28 openings - with an  
863 input data size about 353k points in 35 seconds. This makes this method  
864 faster than the FV method by about 5.5 times for 25 Westmoreland St., and  
865 14.8 times for 6 D'Olier St. (Figure 11c).

866 The method introduced in this paper is limited to reconstructing build-  
867 ing façades and their openings, particularly the windows/doors covered by  
868 low reflectance materials and/or located with a slight recession from exterior  
869 surface of the wall. In the case of solid, wholly openings with no recessed por-  
870 tions, additional attributes of the point cloud, known as the laser backscatter  
871 intensity or red-green-blue colour of the point cloud could be used to estab-  
872 lish the threshold that distinguishes between the points of the wall and those  
873 of the window/door areas.

874 Generated BEPS models from the proposed work flow contain accurate  
875 representations of such façades but do not yet include detailed interior rep-  
876 resentations of the building. A higher LoD for the building, e.g. LoD 4  
877 offers significant potential for comprehensive representation of the building  
878 geometry which can be transformed into BEPS models. This still presents a  
879 significant challenge in terms of data acquisition and processing. A complete  
880 representation of the building could be achieved by integrating data from  
881 other sources, for example: aerial laser scanning or unmanned vehicle aerial  
882 based laser scanning/images, which can provide point clouds for building  
883 roofs and other parts that remain inaccessible to TLS from the ground.

884 Although the TLS has often been used to capture internal building ele-  
885 ments [19], the method requires significant labour on site because the com-  
886 plexity of the building and obstructions from furniture necessitates a large  
887 number of scan stations. In addition, it requires huge effort to register data  
888 points from the large number of the scan stations and to clean irrelevant  
889 data points. To reduce such overheads, a possible solution is to use a robot  
890 with a scanner or a backpack scanner [23]. The advantage of these units is  
891 to reduce time for setting up scan stations, which takes a large portion of  
892 operating time for today's modern scanners, for target acquisition, and office  
893 labour for data registration.

894 In terms of data processing, the data set may contain up to a billion  
895 points and be gigabytes in size. Such data will require new, efficient indexing  
896 and management. Additionally, new, efficient and robust methods should  
897 be developed to extract and reconstruct internal walls, floors, ceilings and  
898 other building components. Existing methods are limited to extracting and  
899 reconstructing planar objects or separate rooms. For example, Okorn et al.

900 [77] succeeded in extracting flat floors and ceilings from a point cloud, while  
901 Turner et. al. (2015) generated models for separate rooms [78]. Further  
902 information (e.g. the thickness of the walls or floors, the types of building  
903 component material) should ideally also be automatically determined from  
904 sensing data, to improve the automation of the pipeline transforming sensed  
905 data into a BEPS model.

906 Although the sensitivity analysis performed in this paper shows that rudi-  
907 mentary geometric models derived from a point cloud differed by approxi-  
908 mately 1% compared to equivalent models from reference data, it is clear  
909 that such discrepancies in geometry do not significantly impact estimations of  
910 building energy usage. Similar analysis needs to be performed and validated  
911 in a more comprehensive evaluation that considers a complete representation  
912 of building geometries. Such experimentation would help to remove uncer-  
913 tainty with respect to the contribution of building geometry to the overall  
914 "performance gap" issue in buildings.

## 915 **6. Conclusions and Future Work**

916 The generation of input data for energy simulation purposes has been a  
917 time-consuming and laborious task, particularly the collection and process-  
918 ing of building geometry information. Laser scanning data provides highly  
919 detailed topographic information for a building, which can provide an oppor-  
920 tunity to generate 3D building models quickly and accurately in a automated  
921 fashion. The models can be used as a basis for BEPS model inputs by adding  
922 further manual inputs not just for one-off projects but as a scalable solution  
923 that is applicable to the majority of the existing urban building stock.

924 This paper describes a semi-automated process whereby point cloud data  
925 captured by TLS is automatically transformed into usable geometric format  
926 for a specific BEPS tool, EnergyPlus. The semi-automated process sub-  
927 sequently requires manual input of basic semantic information for a given  
928 building. The work demonstrates a worthwhile and potentially scalable so-  
929 lution applicable to existing buildings. In this process, utmost care must be  
930 taken when scanning multiple building storeys from a fixed horizontal plane  
931 as scanning inaccuracies can have a downstream impact on building energy  
932 performance prediction.

933 BEPS has an important role to play in the renovation of the exist-  
934 ing building stock by enabling the rapid creation of simulation models in a

935 semi-automated manner. If the costs of creating these models are signifi-  
936 cantly reduced, owners and operators will be better able to cost-effectively  
937 use simulation tools as standard practice for retrofit scenario modelling.

938 Future work in this area includes the extension of this technique to cap-  
939 ture an entire building (exterior and interior objects) and to generate more  
940 complicated structures and building elements such as roofs, free-form sur-  
941 faces, internal objects (e.g. ceiling, internal walls), shading elements, façades  
942 of non-terraced buildings, and skyscrapers. The integration of terrestrial and  
943 aerial point data clouds may also benefit 3D building models with LoD 4 by  
944 facilitating the coupling of exterior and interior building models. Finally,  
945 the transformation of point clouds to BIM and GIS based formats offers the  
946 potential for simulation at neighbourhood, district, and city scales.

## 947 7. Acknowledgements

948 This work was supported by a Marie Curie FP7 Integration Grant within  
949 the 7th European Union Framework Programme project title SuPerB, project  
950 number 631617. The third and last authors are grateful the generous sup-  
951 port of the European Commission through FP7 ERC Consolidator grant,  
952 “RETURN: Rethinking Tunnelling for Urban Neighbourhoods”), ERC StG  
953 2012-307836-RETURN. The authors would like Cathal Hoare for proof read-  
954 ing the final manuscript.

## 955 8. References

- 956 [1] T. A. Reddy, I. Maor, C. Panjapornpon, Calibrating detailed build-  
957 ing energy simulation programs with measured data—part i: Gen-  
958 eral methodology (rp-1051), *Hvac&R Research* 13 (2) (2007) 221–241.  
959 doi:10.1080/10789669.2007.10390952.
- 960 [2] C. Turner, Frankel, Energy Performance of LEED for New Construc-  
961 tion Buildings, Final Final Version, New Buildings Institute, PO Box  
962 2349 White Salmon, WA 98672 509-493-4468 1331 Washington Street  
963 Vancouver, WA 98660 (Mar. 2008).  
964 URL [https://www.usgbc.org/drupal/legacy/usgbc/docs/  
965 Archive/General/Docs3930.pdf](https://www.usgbc.org/drupal/legacy/usgbc/docs/Archive/General/Docs3930.pdf)
- 966 [3] J. H. Scofield, Do LEED-certified buildings save energy? Not  
967 really..., *Energy and Buildings* 41 (12) (2009) 1386 – 1390.



- 968 doi:10.1016/j.enbuild.2009.08.006.  
969 URL [http://www.sciencedirect.com/science/article/pii/  
970 S037877880900187X](http://www.sciencedirect.com/science/article/pii/S037877880900187X)
- 971 [4] P. de Wilde, R. Jones, The building energy performance gap: Up close  
972 and personal, in: CIBSE ASHRAE Technical Symposium: Moving to a  
973 new world of building systems performance, 2014, pp. 1–12.  
974 URL [https://www.cibse.org/technical-symposium-2019/  
975 past-papers-case-studies-archive/2014](https://www.cibse.org/technical-symposium-2019/past-papers-case-studies-archive/2014)
- 976 [5] A. C. Menezes, A. Cripps, D. Bouchlaghem, R. Buswell, Predicted  
977 vs. actual energy performance of non-domestic buildings: Using  
978 post-occupancy evaluation data to reduce the performance gap, Energy  
979 Solutions for a Sustainable World - Proceedings of the Third Interna-  
980 tional Conference on Applied Energy, May 16-18, 2011 - Perugia, Italy  
981 97 (0) (2012) 355–364. doi:10.1016/j.apenergy.2011.11.075.  
982 URL [http://www.sciencedirect.com/science/article/pii/  
983 S0306261911007811](http://www.sciencedirect.com/science/article/pii/S0306261911007811)
- 984 [6] J. O’Donnell, M. Keane, E. Morrissey, V. Bazjanac, Scenario modelling:  
985 A holistic environmental and energy management method for building  
986 operation optimisation, Energy and Buildings 62 (2013) 146–157.  
987 doi:10.1016/j.enbuild.2012.10.060.  
988 URL [http://www.sciencedirect.com/science/article/pii/  
989 S0378778813001345](http://www.sciencedirect.com/science/article/pii/S0378778813001345)
- 990 [7] D. Coakley, E. Corry, M. Keane, Validation of Simulated Thermal Com-  
991 fort using a Calibrated Building Energy Simulation (BES) model in  
992 the context of Building Performance Evaluation & Optimisation, in:  
993 13th annual International Conference for Enhanced Building Opera-  
994 tions (ICEBO), Energy Systems Laboratory, Texas A&M University  
995 (<http://www.tamu.edu>), 2013, pp. 1–12.  
996 URL <http://hdl.handle.net/1969.1/151416>
- 997 [8] I. Z. Bribián, A. A. Usón, O. S. Cardaño, A. Munar, Development of  
998 European Ecolabel and Green Public Procurement Criteria for Office  
999 Buildings JRC IPTS Draft Report, Tech. rep., Joint Research Center  
1000 European Commission, Seville, Spain (Jun. 2011).  
1001 URL [http://susproc.jrc.ec.europa.eu/buildings/docs/  
1002 product%20definition%20and%20scope.pdf](http://susproc.jrc.ec.europa.eu/buildings/docs/product%20definition%20and%20scope.pdf)

- 1003 [9] P. de Wilde, The gap between predicted and measured energy perfor-  
1004 mance of buildings: A framework for investigation, *Automation in Con-*  
1005 *struction* 41 (1) (2014) 40–49. doi:10.1016/j.autcon.2014.02.009.  
1006 URL [http://www.sciencedirect.com/science/article/pii/](http://www.sciencedirect.com/science/article/pii/S092658051400034X)  
1007 [S092658051400034X](http://www.sciencedirect.com/science/article/pii/S092658051400034X)
- 1008 [10] Y. K. Cho, Y. Ham, M. Golpavar-Fard, 3D as-is building energy  
1009 modeling and diagnostics: A review of the state-of-the-art, *Advanced*  
1010 *Engineering Informatics* 29 (2) (2015) 184 – 195, *infrastructure Com-*  
1011 *puter Vision*. doi:10.1016/j.aei.2015.03.004.  
1012 URL [http://www.sciencedirect.com/science/article/pii/](http://www.sciencedirect.com/science/article/pii/S1474034615000312)  
1013 [S1474034615000312](http://www.sciencedirect.com/science/article/pii/S1474034615000312)
- 1014 [11] J. Jung, S. Hong, S. Jeong, S. Kim, H. Cho, S. Hong, J. Heo,  
1015 Productive modeling for development of as-built BIM of existing  
1016 indoor structures, *Automation in Construction* 42 (0) (2014) 68 – 77.  
1017 doi:10.1016/j.autcon.2014.02.021.  
1018 URL [http://www.sciencedirect.com/science/article/pii/](http://www.sciencedirect.com/science/article/pii/S0926580514000466)  
1019 [S0926580514000466](http://www.sciencedirect.com/science/article/pii/S0926580514000466)
- 1020 [12] F. Bosché, M. Ahmed, Y. Turkan, C. T. Haas, R. Haas, The value of  
1021 integrating Scan-to-BIM and Scan-vs-BIM techniques for construction  
1022 monitoring using laser scanning and BIM: The case of cylindrical  
1023 {MEP} components, *Automation in Construction* 49 Part B (1) (2015)  
1024 201–213. doi:10.1016/j.autcon.2014.05.014.  
1025 URL [http://www.sciencedirect.com/science/article/pii/](http://www.sciencedirect.com/science/article/pii/S0926580514001319)  
1026 [S0926580514001319](http://www.sciencedirect.com/science/article/pii/S0926580514001319)
- 1027 [13] C. Früh, A. Zakhor, An Automated Method for Large-Scale, Ground-  
1028 Based City Model Acquisition, *International Journal of Computer Vision*  
1029 60 (1) (2004) 5–24. doi:10.1023/B:VISI.0000027787.82851.b6.  
1030 URL <http://dx.doi.org/10.1023/B%3AVISI.0000027787.82851.b6>
- 1031 [14] V. Bazjanac, Acquisition of Building Geometry in the Simulation of  
1032 Energy Performance, in: 7th International IBPSA Conference Building  
1033 Simulation 2001, IBPSA ISSN 2522-2708, Rio de Janeiro, Brazil, 2001,  
1034 pp. 305–312.  
1035 URL [http://www.ibpsa.org/proceedings/BS2001/BS01\\_0305\\_312.](http://www.ibpsa.org/proceedings/BS2001/BS01_0305_312.pdf)  
1036 [pdf](http://www.ibpsa.org/proceedings/BS2001/BS01_0305_312.pdf)

- 1037 [15] J. O'Donnell, T. Maile, C. Rose, N. Mrazović, E. Morrissey, C. Regnier,  
1038 K. Parrish, V. Bazjanac, Transforming BIM to BEM: Generation of  
1039 Building Geometry for the NASA Ames Sustainability Base BIM, Tech.  
1040 Rep. LBNL-6033E, LBNL (2013).  
1041 URL <http://eetd.lbl.gov/node/51468>
- 1042 [16] C. M. Rose, V. Bazjanac, An algorithm to generate space boundaries  
1043 for building energy simulation, *Engineering with Computers* 31 (2015)  
1044 271–280. doi:10.1007/s00366-013-0347-5.  
1045 URL <http://link.springer.com/10.1007/s00366-013-0347-5>
- 1046 [17] C. van Treeck, E. Rank, Dimensional reduction of 3d building  
1047 models using graph theory and its application in building energy  
1048 simulation, *Engineering with Computers* 23 (2) (2007) 109–122.  
1049 doi:10.1007/s00366-006-0053-7.  
1050 URL <http://link.springer.com/article/10.1007/s00366-006-0053-7>  
1051
- 1052 [18] T. L. Garwood, B. R. Hughes, D. O'Connor, J. K. Calautit,  
1053 M. R. Oates, T. Hodgson, A framework for producing gbXML  
1054 building geometry from Point Clouds for accurate and efficient  
1055 Building Energy Modelling, *Applied Energy* 224 (2018) 527–537.  
1056 doi:10.1016/j.apenergy.2018.04.046.  
1057 URL <http://www.sciencedirect.com/science/article/pii/S0306261918306044>  
1058
- 1059 [19] T. L. Garwood, B. R. Hughes, D. O'Connor, J. K. Calautit, M. R.  
1060 Oates, T. Hodgson, Geometry Extraction for High Resolution Building  
1061 Energy Modelling Applications from Point Cloud Data: A Case  
1062 Study of a Factory Facility, *Energy Procedia* 142 (2017) 1805–1810.  
1063 doi:10.1016/j.egypro.2017.12.567.  
1064 URL <http://www.sciencedirect.com/science/article/pii/S1876610217363233>  
1065
- 1066 [20] A. Budroni, J. Böhm, Toward automatic reconstruction of interiors from  
1067 laser data, in: *Proceedings of Virtual Reconstruction and Visualization*  
1068 *of Complex Architectures (3D-Arch)*, ISPRS, p. 7.  
1069 URL [https://www.isprs.org/proceedings/XXXVIII/5-W1/pdf/budroni\\_boehm.pdf](https://www.isprs.org/proceedings/XXXVIII/5-W1/pdf/budroni_boehm.pdf)  
1070

- 1071 [21] E. Valero, A. Adán, C. Cerrada, Automatic method for building indoor  
1072 boundary models from dense point clouds collected by laser scanners,  
1073 *Sensors* 12 (12) (2012) 16099–16115. doi:10.3390/s121216099.  
1074 URL <http://www.mdpi.com/1424-8220/12/12/16099>
- 1075 [22] V. Sanchez, A. Zakhor, Planar 3D modeling of building interiors from  
1076 point cloud data, in: 19th IEEE International Conference on Image  
1077 Processing, 2012, pp. 1777–1780. doi:10.1109/ICIP.2012.6467225.
- 1078 [23] W. Shi, W. Ahmed, N. Li, W. Fan, H. Xiang, M. Wang, Semantic  
1079 Geometric Modelling of Unstructured Indoor Point Cloud, *ISPRS In-*  
1080 *ternational Journal of Geo-Information* 8 (1) (2019) 9. doi:10.3390/  
1081 *ijgi8010009*.  
1082 URL <https://www.mdpi.com/2220-9964/8/1/9>
- 1083 [24] V. Bazjanac, T. Maile, C. Nytsch-Geusen, Generation of building ge-  
1084 ometry for energy performance simulation using Modelica, in: *BauSim*  
1085 *Conference, Dresden, Germany, 2016*, pp. 361–368.  
1086 URL [http://www.ibpsa.org/proceedings/bausimPapers/2016/](http://www.ibpsa.org/proceedings/bausimPapers/2016/D-01-1.pdf)  
1087 [D-01-1.pdf](http://www.ibpsa.org/proceedings/bausimPapers/2016/D-01-1.pdf)
- 1088 [25] Y. Ham, M. Golparvar-Fard, An automated vision-based method for  
1089 rapid 3d energy performance modeling of existing buildings using  
1090 thermal and digital imagery, *Advanced Engineering Informatics* 27 (3)  
1091 (2013) 395–409. doi:10.1016/j.aei.2013.03.005.  
1092 URL [http://www.sciencedirect.com/science/article/pii/](http://www.sciencedirect.com/science/article/pii/S147403461300027X)  
1093 [S147403461300027X](http://www.sciencedirect.com/science/article/pii/S147403461300027X)
- 1094 [26] Technical University Berlin, Energy Atlas Berlin, [Accessed 2-10-2018]  
1095 (2015).  
1096 URL <http://energyatlas.energie.tu-berlin.de/>
- 1097 [27] L. Madrazo, SEMANCO, [Accessed 2-10-2018] (2015).  
1098 URL <http://www.semanco-project.eu/>
- 1099 [28] S. L. López, J. C. García, J. M. Sánchez, D. R. Bernárdez, H. L.  
1100 Cimadevila, Thermographic mobile mapping of urban environment for  
1101 lighting and energy studies, *Journal of Daylighting* 1 (1) (2014) 8–15.  
1102 doi:10.15627/jd.2014.2.

- 1103 [29] K. Maragkogiannis, D. Kolokotsa, E. Maravelakis, A. Konstanta-  
1104 ras, Combining terrestrial laser scanning and computational fluid  
1105 dynamics for the study of the urban thermal environment, *Sus-  
1106 tainable Cities and Society* 13 (Supplement C) (2014) 207 – 216.  
1107 doi:10.1016/j.scs.2013.12.002.  
1108 URL [http://www.sciencedirect.com/science/article/pii/  
1109 S2210670713000851](http://www.sciencedirect.com/science/article/pii/S2210670713000851)
- 1110 [30] S. Lagüela, J. Martínez, J. Armesto, P. Arias, Energy effi-  
1111 ciency studies through 3D laser scanning and thermographic  
1112 technologies, *Energy and Buildings* 43 (6) (2011) 1216 – 1221.  
1113 doi:<https://doi.org/10.1016/j.enbuild.2010.12.031>.  
1114 URL [http://www.sciencedirect.com/science/article/pii/  
1115 S0378778811000041](http://www.sciencedirect.com/science/article/pii/S0378778811000041)
- 1116 [31] D. González-Aguilera, S. Lagüela, P. Rodríguez-Gonzálvez,  
1117 D. Hernández-López, Image-based thermographic modeling for assessing  
1118 energy efficiency of buildings façades, *Energy and Buildings* 65 (Sup-  
1119 plement C) (2013) 29 – 36. doi:10.1016/j.enbuild.2013.05.040.  
1120 URL [http://www.sciencedirect.com/science/article/pii/  
1121 S0378778813003289](http://www.sciencedirect.com/science/article/pii/S0378778813003289)
- 1122 [32] S. Lagüela, L. Díaz-Vilariño, J. Martínez, J. Armesto, Automatic  
1123 thermographic and RGB texture of as-built BIM for energy rehabili-  
1124 tation purposes, *Automation in Construction* 31 (0) (2013) 230 – 240.  
1125 doi:10.1016/j.autcon.2012.12.013.  
1126 URL [http://www.sciencedirect.com/science/article/pii/  
1127 S092658051200252X](http://www.sciencedirect.com/science/article/pii/S092658051200252X)
- 1128 [33] D. Borrmann, A. Nüchter, M. Đakulović, I. Maurović, I. Petrović,  
1129 D. Osmanković, J. Velagić, A mobile robot based system for fully  
1130 automated thermal 3D mapping, *Advanced Engineering Informatics*  
1131 28 (4) (2014) 425 – 440. doi:10.1016/j.aei.2014.06.002.  
1132 URL [http://www.sciencedirect.com/science/article/pii/  
1133 S1474034614000408](http://www.sciencedirect.com/science/article/pii/S1474034614000408)
- 1134 [34] Y. Cho, C. Wang, 3D thermal modeling for existing buildings using  
1135 hybrid LIDAR system, in: *Computing in Civil Engineering* (2011),  
1136 Miami, Florida, pp. 552–559. doi:10.1061/41182(416)68.

- 1137 URL [https://ascelibrary.org/doi/abs/10.1061/41182%28416%](https://ascelibrary.org/doi/abs/10.1061/41182%28416%2968)  
1138 2968
- 1139 [35] F. Moran, T. Blight, S. Natarajan, A. Shea, The use of passive house  
1140 planning package to reduce energy use and CO<sub>2</sub> emissions in historic  
1141 dwellings, *Energy and Buildings* 75 (Supplement C) (2014) 216 – 227.  
1142 doi:10.1016/j.enbuild.2013.12.043.  
1143 URL [http://www.sciencedirect.com/science/article/pii/](http://www.sciencedirect.com/science/article/pii/S0378778813008608)  
1144 S0378778813008608
- 1145 [36] M. Morelli, L. Rønby, S. E. Mikkelsen, M. G. Minzari, T. Kildemoes,  
1146 H. M. Tommerup, Energy retrofitting of a typical old danish multi-  
1147 family building to a “nearly-zero” energy building based on experiences  
1148 from a test apartment, *Energy and Buildings* 54 (Supplement C) (2012)  
1149 395 – 406. doi:<https://doi.org/10.1016/j.enbuild.2012.07.046>.  
1150 URL [http://www.sciencedirect.com/science/article/pii/](http://www.sciencedirect.com/science/article/pii/S0378778812004021)  
1151 S0378778812004021
- 1152 [37] Y. Ham, M. Golparvar-Fard, Mapping actual thermal properties to  
1153 building elements in gbXML-based BIM for reliable building energy  
1154 performance modeling, *Automation in Construction* 49, Part B (2015)  
1155 214–224. doi:10.1016/j.autcon.2014.07.009.  
1156 URL [http://www.sciencedirect.com/science/article/pii/](http://www.sciencedirect.com/science/article/pii/S0926580514001605)  
1157 S0926580514001605
- 1158 [38] L. Truong-Hong, D. F. Laefer, T. Hinks, H. Carr, Flying Voxel Method  
1159 with Delaunay Triangulation Criterion for Façades/Feature Detection  
1160 for Computation, *Journal of Computing in Civil Engineering* 26 (6)  
1161 (2012) 691–707. doi:10.1061/(ASCE)CP.1943-5487.0000188.  
1162 URL [http://ascelibrary.org/doi/abs/10.1061/%28ASCE%29CP.](http://ascelibrary.org/doi/abs/10.1061/%28ASCE%29CP.1943-5487.0000188)  
1163 1943-5487.0000188
- 1164 [39] S. Pu, G. Vosselman, Knowledge based reconstruction of building mod-  
1165 els from terrestrial laser scanning data, *ISPRS Journal of Photogram-*  
1166 *metry and Remote Sensing* 64 (6) (2009) 575–584. doi:10.1016/j.  
1167 isprsjprs.2009.04.001.  
1168 URL [https://www.sciencedirect.com/science/article/abs/pii/](https://www.sciencedirect.com/science/article/abs/pii/S0924271609000501)  
1169 S0924271609000501

- 1170 [40] L. Díaz-Vilariño, S. Lagüela, J. Armesto, P. Arias, Indoor daylight simu-  
1171 lation performed on automatically generated as-built 3D models, *Energy*  
1172 and *Buildings* 68 (2014) 54–62. doi:10.1016/j.enbuild.2013.02.064.  
1173 URL [https://www.sciencedirect.com/science/article/pii/  
1174 S0378778813006038](https://www.sciencedirect.com/science/article/pii/S0378778813006038)
- 1175 [41] S. M. Iman Zolanvari, D. F. Laefer, Slicing Method for curved  
1176 façade and window extraction from point clouds, *ISPRS Jour-*  
1177 *nal of Photogrammetry and Remote Sensing* 119 (2016) 334–346.  
1178 doi:10.1016/j.isprsjprs.2016.06.011.  
1179 URL [http://www.sciencedirect.com/science/article/pii/  
1180 S0924271616301228](http://www.sciencedirect.com/science/article/pii/S0924271616301228)
- 1181 [42] J. Li, B. Xiong, F. Biljecki, G. Schrotter, A sliding window method  
1182 for detecting corners of openings from terrestrial lidar data, *ISPRS*  
1183 *- International Archives of the Photogrammetry, Remote Sens-*  
1184 *ing and Spatial Information Sciences XLII-4/W10* (2018) 97–103.  
1185 doi:10.5194/isprs-archives-XLII-4-W10-97-2018.  
1186 URL [https://www.int-arch-photogramm-remote-sens-spatial-inf-sci.  
1187 net/XLII-4-W10/97/2018/](https://www.int-arch-photogramm-remote-sens-spatial-inf-sci.net/XLII-4-W10/97/2018/)
- 1188 [43] J. Jung, C. Stachniss, S. Ju, J. Heo, Automated 3d volumet-  
1189 ric reconstruction of multiple-room building interiors for as-  
1190 built BIM, *Advanced Engineering Informatics* 38 (2018) 811–825.  
1191 doi:10.1016/j.aei.2018.10.007.  
1192 URL [http://www.sciencedirect.com/science/article/pii/  
1193 S1474034618300600](http://www.sciencedirect.com/science/article/pii/S1474034618300600)
- 1194 [44] A. Adan, D. Huber, 3D reconstruction of interior wall surfaces under  
1195 occlusion and clutter, in: *2011 International Conference on 3D Imaging,*  
1196 *Modeling, Processing, Visualization and Transmission, IEEE, 2011, pp.*  
1197 *275–281.* doi:10.1109/3DIMPVT.2011.42.
- 1198 [45] C. Wang, Y. K. Cho, Automatic as-is 3D building models creation from  
1199 unorganized point clouds, in: *Construction Research Congress 2014,*  
1200 *2014, pp. 917–924.* doi:10.1061/9780784413517.094.  
1201 URL [https://ascelibrary.org/doi/abs/10.1061/9780784413517.  
1202 094](https://ascelibrary.org/doi/abs/10.1061/9780784413517.094)

- 1203 [46] J. Jung, S. Hong, S. Yoon, J. Kim, J. Heo, Automated 3d wireframe  
1204 modeling of indoor structures from point clouds using constrained least-  
1205 squares adjustment for as-built bim, *Journal of Computing in Civil*  
1206 *Engineering* 30 (4) (2016) 04015074. arXiv:[https://ascelibrary.](https://ascelibrary.org/doi/pdf/10.1061/\%28ASCE\%29CP.1943-5487.0000556)  
1207 [org/doi/pdf/10.1061/\%28ASCE\%29CP.1943-5487.0000556](https://ascelibrary.org/doi/pdf/10.1061/\%28ASCE\%29CP.1943-5487.0000556),  
1208 doi:10.1061/(ASCE)CP.1943-5487.0000556.  
1209 URL [https://ascelibrary.org/doi/abs/10.1061/\%28ASCE\%29CP.](https://ascelibrary.org/doi/abs/10.1061/\%28ASCE\%29CP.1943-5487.0000556)  
1210 [1943-5487.0000556](https://ascelibrary.org/doi/abs/10.1061/\%28ASCE\%29CP.1943-5487.0000556)
- 1211 [47] M. Tamke, H. L. Evers, M. Zwierzycki, R. Wessel, S. Ochmann,  
1212 R. Vock, R. Klein, An automated approach to the generation of  
1213 structured building information models from unstructured 3d point  
1214 cloud scans, in: *Proceedings of IASS Annual Symposia, Vol. 2016,*  
1215 *International Association for Shell and Spatial Structures (IASS), 2016,*  
1216 pp. 1–10.  
1217 URL [https://adk.elsevierpure.com/en/publications/](https://adk.elsevierpure.com/en/publications/an-automated-approach-to-the-generation-of-structured-building-in)  
1218 [an-automated-approach-to-the-generation-of-structured-building-in](https://adk.elsevierpure.com/en/publications/an-automated-approach-to-the-generation-of-structured-building-in)
- 1219 [48] S. Ochmann, R. Vock, R. Wessel, R. Klein, Automatic reconstruction  
1220 of parametric building models from indoor point clouds, *Computers &*  
1221 *Graphics* 54 (2016) 94–103. doi:10.1016/j.cag.2015.07.008.  
1222 URL [http://www.sciencedirect.com/science/article/pii/](http://www.sciencedirect.com/science/article/pii/S0097849315001119)  
1223 [S0097849315001119](http://www.sciencedirect.com/science/article/pii/S0097849315001119)
- 1224 [49] B. Quintana, S. A. Prieto, A. Adán, F. Bosché, Door detection in 3d  
1225 coloured point clouds of indoor environments, *Automation in Construc-*  
1226 *tion* 85 (2018) 146–166. doi:10.1016/j.autcon.2017.10.016.  
1227 URL [http://www.sciencedirect.com/science/article/pii/](http://www.sciencedirect.com/science/article/pii/S0926580516302400)  
1228 [S0926580516302400](http://www.sciencedirect.com/science/article/pii/S0926580516302400)
- 1229 [50] B. Staats, A. Diakit , R. Vo te, S. Zlatanova, Detection of doors in a  
1230 voxel model, derived from a point cloud and its scanner trajectory, to  
1231 improve the segmentation of the walkable space, *International Journal*  
1232 *of Urban Sciences* (2018) 1–22doi:10.1080/12265934.2018.1553685.  
1233 URL <https://doi.org/10.1080/12265934.2018.1553685>
- 1234 [51] L. Li, F. Su, F. Yang, H. Zhu, D. Li, X. Zuo, F. Li, Y. Liu, S. Ying, Re-  
1235 construction of Three-Dimensional (3d) Indoor Interiors with Multiple  
1236 Stories via Comprehensive Segmentation, *Remote Sensing* 10 (8) (2018)



- 1237 1281. doi:10.3390/rs10081281.  
1238 URL <https://www.mdpi.com/2072-4292/10/8/1281>
- 1239 [52] H. Tran, K. Khoshelham, A. Kealy, L. Díaz-Vilariño, Shape grammar  
1240 approach to 3d modeling of indoor environments using point clouds,  
1241 Journal of Computing in Civil Engineering 33 (1) (2018) 04018055.  
1242 doi:10.1061/(ASCE)CP.1943-5487.0000800.  
1243 URL [https://ascelibrary.org/doi/10.1061/%28ASCE%29CP.  
1244 1943-5487.0000800](https://ascelibrary.org/doi/10.1061/%28ASCE%29CP.1943-5487.0000800)
- 1245 [53] C. Wang, S. Hou, C. Wen, Z. Gong, Q. Li, X. Sun, J. Li, Semantic  
1246 line framework-based indoor building modeling using backpacked laser  
1247 scanning point cloud, ISPRS Journal of Photogrammetry and Remote  
1248 Sensing 143 (2018) 150–166. doi:10.1016/j.isprsjprs.2018.03.025.  
1249 URL [http://www.sciencedirect.com/science/article/pii/  
1250 S092427161830090X](http://www.sciencedirect.com/science/article/pii/S092427161830090X)
- 1251 [54] M. Neuhausen, M. König, Automatic window detection in fa-  
1252 cade images, Automation in Construction 96 (2018) 527 – 539.  
1253 doi:<https://doi.org/10.1016/j.autcon.2018.10.007>.  
1254 URL [http://www.sciencedirect.com/science/article/pii/  
1255 S092658051830551X](http://www.sciencedirect.com/science/article/pii/S092658051830551X)
- 1256 [55] G. Gröger, T. Kolbe, C. Nagel, K. Hafele, OpenGIS City Geography  
1257 Markup Language (CityGML) Encoding Standard (OGC 12-019). Ver-  
1258 sion 2.0.0. OGC 12-019., last accessed 2014-11-03 (2014).  
1259 URL <http://www.opengeospatial.org/standards/citygml>
- 1260 [56] Trimble Navigation Limited, RealWork Survey Advanced, last accessed  
1261 2014-11-03 (2014).  
1262 URL [https://geospatial.trimble.com/products-and-solutions/  
1263 trimble-realworks](https://geospatial.trimble.com/products-and-solutions/trimble-realworks)
- 1264 [57] T. Rabbani, F. van den Heuvel, G. Vosselman, Segmentation of point  
1265 clouds using smoothness constraints, in: H. Maas, D. Schneider (Eds.),  
1266 ISPRS 2006 : Proceedings of the ISPRS commission V symposium Vol.  
1267 35, part 6 : image engineering and vision metrology, Dresden, Germany  
1268 25-27 September 2006, Vol. 35, ISSN 1682-1750, International Society  
1269 for Photogrammetry and Remote Sensing (ISPRS), 2006, pp. 248–253.

- 1270 [58] R. Schnabel, R. Wahl, R. Klein, Efficient ransac for point-cloud shape  
1271 detection, *Computer Graphics Forum* 26 (2) (2007) 214–226.  
1272 URL [http://cg.cs.uni-bonn.de/en/publications/  
1273 paper-details/schnabel-2007-efficient/](http://cg.cs.uni-bonn.de/en/publications/paper-details/schnabel-2007-efficient/)
- 1274 [59] A.-V. Vo, L. Truong-Hong, D. F. Laefer, M. Bertolotto, Octree-  
1275 based region growing for point cloud segmentation, *{ISPRS} Journal  
1276 of Photogrammetry and Remote Sensing* 104 (2015) 88 – 100.  
1277 doi:<http://dx.doi.org/10.1016/j.isprsjprs.2015.01.011>.  
1278 URL [http://www.sciencedirect.com/science/article/pii/  
1279 S0924271615000283](http://www.sciencedirect.com/science/article/pii/S0924271615000283)
- 1280 [60] H. Hoppe, T. DeRose, T. Duchamp, J. McDonald, W. Stuetzle, Surface  
1281 reconstruction from unorganized points, *SIGGRAPH Comput. Graph.*  
1282 26 (2) (1992) 71–78. doi:10.1145/142920.134011.  
1283 URL <http://doi.acm.org/10.1145/142920.134011>
- 1284 [61] L. Truong-Hong, D. F. Laefer, Octree-based, automatic building façade  
1285 generation from LiDAR data, *Computer-Aided Design* 53 (2014) 46–61.  
1286 doi:10.1016/j.cad.2014.03.001.
- 1287 [62] N. Ripperda, Determination of façade attributes for façade reconstruc-  
1288 tion, *International Archives of Photogrammetry, Remote Sensing and  
1289 Spatial Information Sciences* 37 (B3.a) (2008) 285–290.  
1290 URL [http://www.isprs.org/proceedings/XXXVII/congress/3\\_  
1291 pdf/44.pdf](http://www.isprs.org/proceedings/XXXVII/congress/3_pdf/44.pdf)
- 1292 [63] S. Becker, N. Haala, Refinement of building fassades by integrated  
1293 processing of LIDAR and image data, *International Archives of  
1294 Photogrammetry, Remote Sensing and Spatial Information Science* 36  
1295 (2007) 7–12.  
1296 URL [http://www.ifp.uni-stuttgart.de/publications/2007/  
1297 becker\\_haala\\_pia07.pdf](http://www.ifp.uni-stuttgart.de/publications/2007/becker_haala_pia07.pdf)
- 1298 [64] S. Pu, G. Vosselman, Extracting windows from terrestrial laser scanning,  
1299 in: *ISPRS Workshop on Laser Scanning and SilviLaser*, Espoo, Finland,  
1300 2007, pp. 320–5.  
1301 URL <https://foto.aalto.fi/ls2007/>

- 1302 [65] G. H. Bendels, R. Schnabel, R. Klein, Detecting holes in point set  
1303 surfaces, in: V. Skala (Ed.), The 14<sup>th</sup> International Conference in  
1304 Central Europe on Computer Graphics, Visualization and Computer  
1305 Vision 2006 (WSCG 2006), Vol. 14, UNION Agency-Science Press,  
1306 ISSN 1213-6972, 2006.  
1307 URL [http://cg.cs.uni-bonn.de/aigaion2root/attachments/  
1308 bendels-2006-detecting.pdf](http://cg.cs.uni-bonn.de/aigaion2root/attachments/bendels-2006-detecting.pdf)
- 1309 [66] L. Truong-Hong, D. F. Laefer, T. Hinks, H. Carr, Combining an an-  
1310 gle criterion with voxelization and the flying voxel method in recon-  
1311 structing building models from LiDAR data, Computer-Aided Civil and  
1312 Infrastructure Engineering 28 (2) (2013) 112–129. doi:10.1111/j.  
1313 1467-8667.2012.00761.x.
- 1314 [67] F. Pighin, J. Lewis, Siggraph 2007 course notes  
1315 Practical Least-Squares for Computer Graphics,  
1316 <http://graphics.stanford.edu/jplewis/lscourse/ls.pdf> (2007).
- 1317 [68] P. Tang, B. Akinci, D. Huber, Quantification of edge loss of laser scanned  
1318 data at spatial discontinuities, Automation in Construction 18 (8) (2009)  
1319 1070–1083. doi:10.1016/j.autcon.2009.07.001.
- 1320 [69] D. Belton, D. D. Lichti, Classification and segmentation of terrestrial  
1321 laser scanner point clouds using local variance information, Inter-  
1322 national Archives of Photogrammetry, Remote Sensing and Spatial  
1323 Information Sciences 36 (5) (2006) 44–49.  
1324 URL [http://www.isprs.org/proceedings/xxxvi/part5/paper/  
1325 BELT\\_619.pdf](http://www.isprs.org/proceedings/xxxvi/part5/paper/BELT_619.pdf)
- 1326 [70] US-DOE, EnergyPlus Home Page, 2006.  
1327 URL <http://www.eere.energy.gov/buildings/energyplus/>
- 1328 [71] LBNL, Space Boundary Tool (2013).  
1329 URL [http://simulationresearch.lbl.gov/projects/  
1330 space-boundary-tool](http://simulationresearch.lbl.gov/projects/space-boundary-tool)
- 1331 [72] S. Lagüela, L. Díaz-Vilariño, J. Armesto, P. Arias, Non-destructive  
1332 approach for the generation and thermal characterization of an as-  
1333 built BIM, Construction and Building Materials 51 (2014) 55–61.  
1334 doi:10.1016/j.conbuildmat.2013.11.021.

- 1335 URL [http://linkinghub.elsevier.com/retrieve/pii/](http://linkinghub.elsevier.com/retrieve/pii/S0950061813010428)  
1336 S0950061813010428
- 1337 [73] C. Wang, Y. K. Cho, Automated gbxml-based building model creation  
1338 for thermal building simulation, in: 2014 2nd International Conference  
1339 on 3D Vision, Vol. 2, 2014, pp. 111–117. doi:10.1109/3DV.2014.109.
- 1340 [74] J. New, M. Adams, EnergyPlus performance improvements via JSON  
1341 input refactoring, in: 2018 Building Performance Modeling Conference  
1342 and SimBuild, Chicago, IL, 2018, pp. 320–324.  
1343 URL [https://www.ashrae.org/File%20Library/Conferences/](https://www.ashrae.org/File%20Library/Conferences/Specialty%20Conferences/2018%20Building%20Performance%20Analysis%20Conference%20and%20SimBuild/Papers/C044.pdf)  
1344 [Specialty%20Conferences/2018%20Building%20Performance%](https://www.ashrae.org/File%20Library/Conferences/Specialty%20Conferences/2018%20Building%20Performance%20Analysis%20Conference%20and%20SimBuild/Papers/C044.pdf)  
1345 [20Analysis%20Conference%20and%20SimBuild/Papers/C044.pdf](https://www.ashrae.org/File%20Library/Conferences/Specialty%20Conferences/2018%20Building%20Performance%20Analysis%20Conference%20and%20SimBuild/Papers/C044.pdf)
- 1346 [75] K.-H. Bae, D. D. Lichti, A method for automated registration of unor-  
1347 ganised point clouds, ISPRS Journal of Photogrammetry and Remote  
1348 Sensing 63 (1) (2008) 36 – 54, theme Issue: Terrestrial Laser Scanning.  
1349 doi:<https://doi.org/10.1016/j.isprsjprs.2007.05.012>.  
1350 URL [http://www.sciencedirect.com/science/article/pii/](http://www.sciencedirect.com/science/article/pii/S0924271607000597)  
1351 S0924271607000597
- 1352 [76] K. Hammoudi, F. Dornaika, B. Soheilian, N. Paparoditis, Extracting  
1353 outlined planar clusters of street facades from 3D point clouds, in: 2010  
1354 Canadian Conference on Computer and Robot Vision, IEEE, Ottawa,  
1355 ON, Canada, 2010, pp. 122–129. doi:10.1109/CRV.2010.23.
- 1356 [77] B. Okorn, X. Xiong, B. Akinci, D. Huber, Toward automated modeling  
1357 of floor plans, in: Proceedings of the symposium on 3D data processing,  
1358 visualization and transmission, Vol. 2, 2010.  
1359 URL [https://www.ri.cmu.edu/pub\\_files/2010/5/2009%203DPVT%](https://www.ri.cmu.edu/pub_files/2010/5/2009%203DPVT%20plan%20view%20modeling%20v13%20(resubmitted).pdf)  
1360 [20plan%20view%20modeling%20v13%20\(resubmitted\).pdf](https://www.ri.cmu.edu/pub_files/2010/5/2009%203DPVT%20plan%20view%20modeling%20v13%20(resubmitted).pdf)
- 1361 [78] E. Turner, P. Cheng, A. Zakhor, Fast, automated, scalable generation of  
1362 textured 3D models of indoor environments, IEEE Journal of Selected  
1363 Topics in Signal Processing 9 (3) (2015) 409–421. doi:10.1109/JSTSP.  
1364 2014.2381153.